Analysis of background noise and boats noise detection in coastal areas

Sophia Lennartsson
so6664le-s@student.lu.se

Department of Electrical and Information Technology, Lund University

Supervisor: Fredrik Tufvesson, fredrik.tufvesson@eit.lth.se

Examiner: Ove Edfors, ove.edfors@eit.lth.se

Carried out at IVL - Swedish Environmental Research Institute

Company supervisor:
Torbjörn Johansson, torbjorn.johansson@ivl.se

July 16, 2024

Printed in Sweden
Tryckeriet i E-huset, Lund

Abstract

The underwater noise has a significant negative impact on marine animals. The EU has made efforts to keep noise emission within sustainable limits, but only in regards to boats with Automatic Identification System (AIS). The noise of recreational boats, which are the main noise emitter in coastal areas, is overlooked. Thus, there is a need to quantify the noise emitted by recreational boats and, in the extension, develop models for this noise. This thesis aims to give an overview of how background noise varies at some coastal locations and to quantify the contributions of boat noise based on recordings. In addition, the thesis aims to design an energy detector, evaluate the detector applied to recorded noise, and briefly outline alternative methods to detect boat noise. For background noise and boat noise contribution purposes, a probabilistic power spectral density (PPSD) is used. It is applied to a long window to see the background noise, and to two short windows to be able to see the additional noise that is due to boat passages. The background noise is successfully visualized, and the main contributing factor to similar sound signatures in the PPSDs to visualize background noise in different locations is the geometry of the seabed. A minimum level of boat noise contribution can be found using this method, but it requires the recordings to not include precipitation. The energy detector consisted of a rolling window structure with a short and a long window, to compensate for the shifting background noise. The designed detector could detect about half of the boat passages, but could be improved by only considering a certain frequency range and adapting the threshold to the application. Some alternative methods are to investigate the periodicity in the tones of the boat noise or tonal detection. As a tonal detection algorithm, the Estimation of Signal Parameters via Rotational Invariance Techniques (ESPRIT) algorithm is implemented, but found not to be successful as a detector without the use of Akaike Information Criterion (AIC) or Minimum Description Length (MDL) to set a critical parameter. ESPRIT combined with one of the other algorithms is deemed worthy of further investigation.

Popular Science Summary

Studies have shown that the underwater noise undoubtedly has a negative impact on marine animals. The EU have made efforts to keep the noise emission within sustainable limits, but mainly in regards to commercial freight ships. This means that noise from recreational boats, which are the main noise emitter in coastal areas, are overlooked. The noise from recreational boats is also under-investigated, and there are no estimates of the amount of this type of noise. Therefore, it is important to study the noise generated by recreational boats. By doing so, we can develop models to predict this noise and better assess its impact on the environment.

This thesis aims to give an overview of how the background noise varies at coastal locations and to quantify the boat noise contributions based on underwater recordings. Further, the thesis aims to construct and evaluate a method to detect boat noise in the recordings and briefly outline alternative methods to detect boat noise.

Boat noise consists of broadband noise, for instance caused by propeller cavitation and vibration from the hull, and narrowband tones consisting of a fundamental tone and overtones, with a certain relation between the frequencies of the tones. This leaves three main alternatives when trying to detect boat noise: Utilizing the energy, the tonal components or the frequency relationship between the tones in the boat noise.

A commonly used method of the first alternative is the energy detector, which was used in the thesis. Through some modifications the detector would flag events of increased energy relative to the temporary background energy. Though, the method possessed a difficulty of handling precipitation of varying intensity. Overall, the detector identified about half of the boats, with only a few false detections. However, it could be adjusted based on the specific terms of application.

As an alternative, a classical tonal detection algorithm called ESPRIT (Estimation of signal parameters via rotational invariance techniques) was implemented, and recommended for further investigation, since this method does not possess the weaknesses that the energy detector has, such as the difficulties in case of precipitation. The ESPRIT algorithm identifies the frequencies of the most probable

tones within the noise. It always detects at least one tone, but can not determine the exact number of tones. Thus, in combination with another algorithm that determines if there are more than one tone present in the noise, the conclusion should be that there is a boat present if there is more than one tone.

For the purpose of identifying the background noise and boat noise contribution, another method, a probabilistic method was used. The method calculated the occurrence of different types of noise, or more in detail the combinations of frequency and intensity, and visualized the more common noise, or background noise. The main contributing factors of similar background noise at different locations was the geometry of the seabed. This probabilistic method also quantifies the minimum levels of boat noise, assuming that there are no other noise sources, such as precipitation.

Acknowledgments

I would like to direct my thanks to my supervisors Fredrik Tufvesson and Torbjörn Johansson and Carl Andersson for making this thesis possible. Torbjörn, together with Carl, continually provided valuable ideas, discussions and feedback.

Additionally, I also would like to thank the whole group of Acoustics at IVL for the warm welcome, for everything that I learned from them, and the enjoyable time spent with them.

Last but not least, I would like to extend a thanks to my family and my partner for their endless support throughout the thesis and course of education.

Contents

Acronyms

AIC - Akaike Information Criterion
AIS - Automatic Identification System
ESPRIT - Estimation of Signal Parameters via Rotational Invariance Techniques
MDL - Minimum Description Length
PPSD - Probabilistic Power Spectral Density
PSD - Power Spectral Density
RPM - Revolutions Per Minute
SNR - Signal-to-Noise Ratio
SPL - Sound Pressure Level
UNCLOS - United Nations Convention on the Law of the Sea

Chapter 1

Introduction

This introduction aims to set the thesis in a larger perspective and explain why it was conducted. In addition, the research objectives are stated, as well as contributions to the success of these objectives and the scope of the thesis. Lastly, the thesis outline is reviewed.

1.1 The thesis in a larger context

The marine life is under enormous stress with cumulative stressors such as large-scale fishing, marine pollution and climate change. A significant stressor, yet underexplored, is noise emission, which affects the soundscape and the life cycles of marine life [1].

This thesis aims to study the noise emissions from recreational boats in coastal areas and is part of a larger project that investigates the noise emissions from recreational boats and its impact and proposes actions to reduce noise-induced stress in ecosystems and animals [2]. The project is conducted by IVL, KTH and FOI through funding by Formas.

1.2 Motivation

The general impact of underwater noise on marine animals is evident, and recreational boating specifically constitutes a risk of negative impact [1][3][4]. Due to relatively low attenuation and fast propagation of sound in water, marine animals have evolved sophisticated sound sensory organs and made hearing a key determinant of marine animals' actions. For example, they use hearing for navigation, foraging, and reproduction [1]. Negative effects of noise can be the following, [5] all of which may have fatal consequences:

- stress
- behavioral changes
- masking

- temporal hearing loss
- disorientation

Despite this, the implementation of the policy on noise emissions has progressed slowly, partly due to lack of knowledge of the emissions and its impacts [1]. Since underwater noise and its impact have not been rigorously studied, it is hard to establish holistic and reasonable laws and policies. Researchers describe the knowledge of underwater noise as an urgent need, in order to provide policy makers with a sufficient decision basis to properly address this problem [1]. As recently as 2015, the issue was being ignored by high-level policy initiatives. In 2021, only one of the 10 major international agreements addressing noise included binding criteria. This is happening despite the growing ocean-based economy, which is expected to double by 2030 [1].

The impact of underwater noise has slowly begun to be recognized outside the scientific community. For example, by inclusion of the goals regarding noise emissions in the United Nations Convention on the Law of the Sea (UNCLOS) and the EU's Marine Strategy Framework Directive, which is the binding agreement referred to above. Through that agreement, the EU has set limits of the noise pollution allowed, which are to be supervised by the members themselves.

An increasingly popular tool to estimate and manage the noise levels and control that the limits within the EU are met is to use predictive models [3]. The models are large-scale models based on the Automatic Identification System (AIS), meaning that it is primarily accounting for commercial shipping. However, in shallow coastal areas, the main contributor to noise are recreational boats, which are not considered in the models used by the EU. In this way, the models have been shown to underestimate the noise [3].

In coastal areas close to shipping lanes, recreational boats are also the dominant noise emitter [3]. Shallow coastal areas are key habitats for many marine species, and their potentially extra-sensitive breeding periods tend to overlap with the periods of more activity from recreational boats. Estimated sound predictions based on AIS boats, such as the model used by the EU, therefore both possess a significant risk of underestimating the emitted noise levels and their impacts on marine life [3]. Hence, the need to investigate the noise emissions from recreational boats in coastal areas, its impact and potential means of control is of great importance.

With this in mind - the impact on marine animals and deficient emission control techniques - this study is particularly important, and I hope to provide a foundation for further large-scale investigations and predictions. The importance is further reinforced since it specifically focuses on coastal areas and recreational boats, in contrast to the majority of the very few studies available on underwater noise.

1.3 Aim

This master thesis aims to fill some of the gaps in knowledge about the underwater noise emitted by focusing on recreational boats in shallow, coastal regions. More specifically, the aim is:

Q1: To give an overview of how the background noise varies in different locations and geomorphological conditions, using spectral statistics. Quantify the noise contribution from boats.

Q2: To identify boat noise in recorded underwater noise using a energy detector; a signal processing method - and to evaluate the method based on real data, as well as briefly outline alternative possibilities in detecting boat noise.

The study of methods to capture the noise emitted from recreational boats is important. If a method is proved to be successful it could be useful for larger scale analysis based on measurements of the underwater noise and without relying on data about passing boats, and it is a necessary component in the development of a prediction model of the noise in coastal areas. These predictions could directly, or partially, help the EU members to control whether they really satisfy the noise limits set in the Marine Strategy Framework Directive. Further, it could be used to investigate the complex soundscape in coastal regions, and to gain an better understanding of the impact of the marine animals to set suitable and cost efficient policies.

1.4 Method

The thesis is based on continuous measurements without management of the boat traffic, and only with limited measurements of passing boats previously recorded by IVL, and the methods used are chosen in accordance with and adapted to the data.

Initially an analysis to remove potential bias and a stationarity analysis was done; based on Pearson correlation coefficients and an equality test, to find a suitable window size to apply in the other methods.

To achieve the aim of analyzing background noise and getting an estimate of the boat noise contribution probabilistic power spectral densities and spectrograms were used.

To detect boat passages in the data an adapted version of an energy detector was used. Another approach, utilizing the tones to detect boat noise, was tested through the ESPRIT algorithm. This one could either be applied to the correlation coefficients or on the data.

1.5 Limitations

The focus of the thesis is shallow, coastal areas. As many of the notions, methods and measurements in the field of underwater noise, "shallow" is not properly defined, but will here be used for depth of maximum 20 m. Even though the results in this thesis are assumed to be generalizable for shallow and coastal areas, the data being used is only collected at Vasholmarna, near Lysekil in Sweden, as it is considered a representative coastal area.

This thesis will only focus on the sound characteristics of noise emitted from recreational boats. Any choice of parameters and measurements will be adjusted for this. Thus, frequency ranges that are critical for marine animals and the impacts on marine life will not be considered. In addition, an analysis of the possibilities of regulation of the noise pollution will be outside the scope of this thesis.

1.6 Thesis outline

The structure of the thesis is as follows. **Chapter 2** includes an introduction to the field of underwater noise to provide an understanding of the complexity of the study and relevant considerations of the data. The chapter also gives a review of the methods and theory available for the thesis, which are the foundations of the methods described in **Chapter 3**. **Chapter 4** further describes the results, while **Chapter 5** discusses the interpretation of the results, reliability, method choices and further investigations. The final conclusions are summarized in **Chapter 6**.

Chapter 2

Theory

2.1 Overview of the underwater soundscape

This section includes an overview of underwater acoustics and of the noise contributions, homing in on boat noise. In regards to the complexity of the soundscape an overview and the complexity factors are brought up.

2.1.1 Acoustics

There are two ways of detecting sounds: pressure and particle motion. What is considered a loud noise also depends on hearing frequencies and sensitivities for different frequency ranges, which vary between marine species. Hence, the way of quantifying sound and what calculations are considered useful to give a fair understanding of the noise and its impacts, is dependent on the research aim in question.

Impedance, velocity and absorption are some factors that are relevant in the study of noise. Impedance is a physical property that describes the amount of resistance that a sound wave encounters when it propagates through the medium. Thus, water which has a large impedance, 3500 times greater than air, requires more energy to create noise [6]. Impedance also impacts the amount of reflection of a sound wave when meeting a new medium. At the surface, an underwater sound wave encounters almost perfect reflection. When hitting rock bottom, a lot of the sound wave is reflected, whereas a large amount propagates into the new medium when hitting a sandy seabed. Reflection and absorption add interference and complexity to the soundscape, making the seabed an important component of the soundscape of shallow coastal areas.

The speed of sound in water is 1450-1600 m/s, compared to 340 m/s in air. Due to the high speed in the water, the Doppler effect is minimal. The range in sound speed is rather large and depends on pressure and temperature. The pressure increases linearly with depth and the temperature is, at least during summer, higher near the surface and decreases rapidly until it reaches a constant low temperature; see Figure 2.1 for a conceptual visualization. The temperature can vary locally

and close to clines. This rough velocity scheme gives, due to Huygen's principle, a raise to sound channels at the depths where temperature and pressure contribute to the lowest sound speed. In these channels, the sound can travel a distance of 80 to 100 km [1]. This extreme propagation partly explains why underwater noise can be such a problem for marine fauna, even though the sound channels do not appear in shallow water.

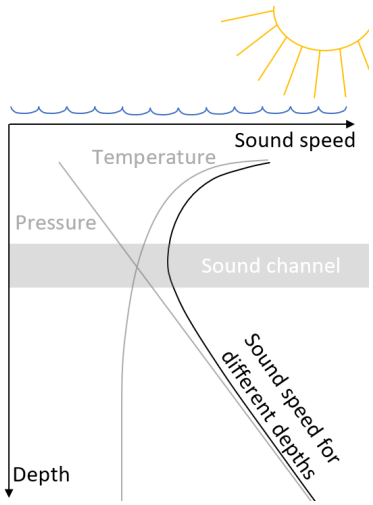

Figure 2.1: A conceptual visualisation of the underwater sound speed and the contribution from the main influence factors, pressure and temperature.

Absorption in water varies around the range of 0.001 to 1 dB / km depending on the frequency [7], where the lower frequencies are less absorbed. This absorption is rather low and explains the very long propagation in water and the problem with a lot of noise in the oceans. Furthermore, shallow water acts as a high pass filter, further influencing the characteristics of sound propagation [3].

2.1.2 Underwater sounds

The underwater sound sources are of biological, geological, meteorological and anthropological character, which partly explains the varying background noise in the seascape. In addition, fast propagation in water, the propagation of lower frequency sounds, the various weather conditions, and the varied depth and seabeds cause varying background noise [8]. The biological noise originates from various sources, such as communication, ecolocation, and unintentional sounds. Geological noise can arise from melting or breaking ice and earthquakes, and antropological sounds often derive from pile driving, boats and explosives [1]. Different sound sources are often characterized by certain sound pressure levels (SPL) for different frequencies, as illustrated in the classical Wenz curves in Figure 2.2.

The main meteorological conditions that affect underwater noise are precipitation and wind. Precipitation causes a clattering sound as drops hit the surface and the

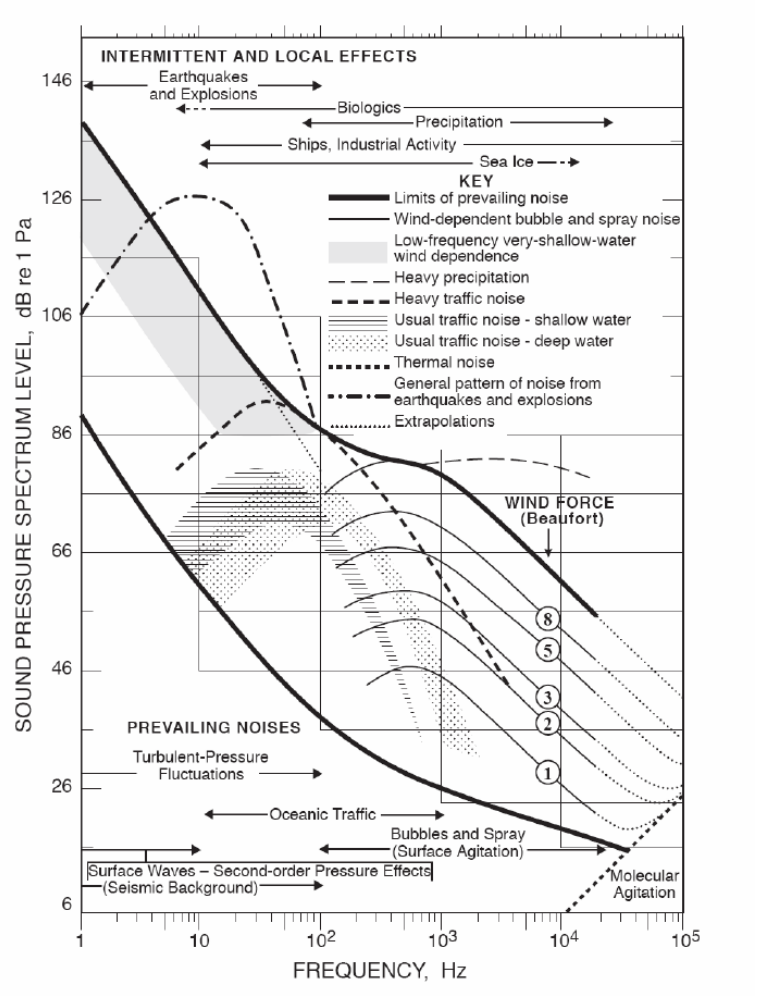

Figure 2.2: Wenz curves showing the SPL and frequency range of different sound sources at sea [9].

wind causes noise through waves that break and crash against the shore. Thus, the impact of the wind assumes the formation of high waves, which was not the case inwards in the archipelago at Vasholmarna.

As seen in Figure 2.2, the contributions of background noise, such as weather and biological noise, often overlap somewhat in frequency and SPL with boat noise, decreasing the signal-to-noise ratio (SNR) of boat noise relative to background noise. Thus, the temporal dimension is important to consider when differentiating the noise types. Among sound sources, one usually distinguishes between impulsive and continuous sounds, where boat noise belongs to the latter category [3].

Boat noise consists of a broadband component and narrowband tones. Broadband

noise mainly comes from the agitation of the surface of the water by the boat, the cavitation of the propeller and the vibration of the hull of the boat [10]. The contribution from the agitation shifts with velocity, since the boat in higher speeds can plane, implying that a smaller amount of water is relocated. The planing velocity in its turn varies with the weight and shape of the boat. Cavitation is the formation of bubbles on the propeller that is caused by low pressure and can appear in different ways. The common is that the cavitation occurs on the propeller and increases with increasing speed. The narrowband tones are due to the motor components, drive shaft and propeller. The tones appear as one fundamental tone, with its frequency corresponding to the revolutions per minute (RPM) and overtones. Depending on the sound level, narrowband tones are sometimes, but not always, the dominant noise source [10].

The spectrogram in Figure 2.3 shows the noise of three distinct boats and the noise caused by rain. The spectrogram shows the time dimension on the x-axis, the frequency dimension on the y-axis and the PSD on the third dimension visualized by a color scheme. The boats appear at 11:13-11:15, 11:17-11:19 and 11:20-11:22, and the rain noise is seen in the frequency range of 300 to 5 000 Hz. As seen, the narrow fundamental tone can be found in a wide range of frequencies. But at least a part of the noise from the measured boat passages is usually within 200 Hz to 10 kHz. The V-shaped form of the tones of the first boat is typical of boat noise and is due to the Lloyd mirror effect [10], [11]. The low magnitude noise in the range of 300 Hz to 5 kHz is due to precipitation. The rest of it is considered background noise.

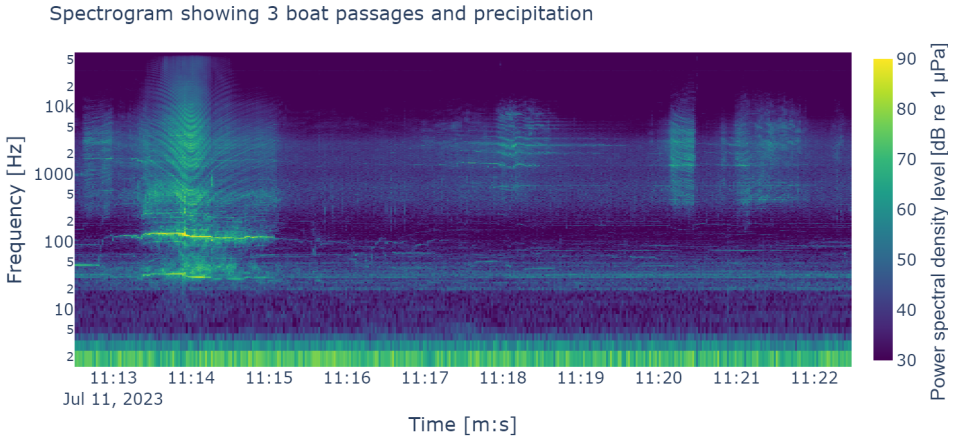

Figure 2.3: Spectrogram visualising the noise of three distinct boats and precipitation noise recorded at Vasholmarna. The power of the frequencies at each time point are given.

2.2 Analysis tools

Given the complex soundscape and shifting background noise, the task of distinguishing the noise from the boat is not easy, and the preferred method varies with the characteristics of the measurements and noise. Some analysis tools that provide a better understanding of the measurements will be reviewed below.

2.2.1 Choise of measurement method and equipment

Just like the seabed, measurement devices can create reflections and hence impact the measurement. A standardized measurement method is therefore of the essence, as the sound level can differ by several dB and can vary differently with respect to the frequencies using different measuring methods. There is no consensus on a standardized measurement of continuous underwater noise, but there are guidelines to achieve regionally consistent measurements [12].

2.2.2 Sound pressure level

SPL is a relative metric that describes the intensity or magnitude of sound and is often used to describe continuous sounds [8]. Due to a large range of hearing levels for humans, the scale is logarithmic, and the SPL is given through:

$$L_p = 20 \cdot \log_{10} \frac{p}{p_0};\ \text{dB re } p_0\ \mu\text{Pa}, \tag{2.1}$$

where p_0 is the reference pressure [8], stated as dB relative to p_0µPa. In air, the reference level is 20 µPa as that is the lowest level of audible noise for humans, compared to 1 µPa in water, making dB levels incomparable between mediums. Due to the large variety in hearing levels within the marina fauna, the SPL metric is not specifically adjusted to marine animals but rather a convention.

2.2.3 Power spectral density and spectrogram

As demonstrated by the Wenz curves in Figure 2.2, the signal can be characterized with respect to both frequency and SPL. The power spectral density (PSD) describes the intensity of the signal for each frequency and is suitable for studying continuous sound, often with the intensity given in power level. The power of the signal is given by

$$P = \lim_{N\to\infty} \frac{1}{2N+1} \sum_{n=-N}^{N} |x(n)|^2, \tag{2.2}$$

where N is the period and $x(n)$ is the discrete time signal, so that the sum denotes the energy of the signal. For convenience $x(n)$ can be substituted to $x_N(n) = x(n)w_N(n)$ where $w_N(n)$ is one in the interval $[-N,N]$ and zero elsewhere, and the limits thus extended to $\pm\infty$. Using Parseval's theorem the average power can be rewritten as

$$P = \lim_{N\to\infty} \frac{1}{f_s(2N+1)} \int_{f=-f_s/2}^{f_s/2} |\widehat{x}_N(f)|^2 df, \tag{2.3}$$

where f_s if the sampling frequency, $\widehat{x}_N(f)$ is the Fourier transformed $x_N(t)$ and the sum still indicates the energy. This, describes the relationship between energy in the time and frequency domains. By the Nyquist-Shannon's sampling theorem frequencies that are larger than $f_s/2$ will not be recovered in the signal. Further, the length of the time signal gives the frequency resolution.

The spectrogram is similar to the PSD but additionally visualizes a time dimension, as seen in Figure 2.3. This is achieved by a rolling window structure, as shown in Figure 2.4, where a total window is repeatedly iterated through its subwindows. In each subwindow the PSD is calculated, meaning that the intensity is described for each frequency and for each time stamp at the subwindows.

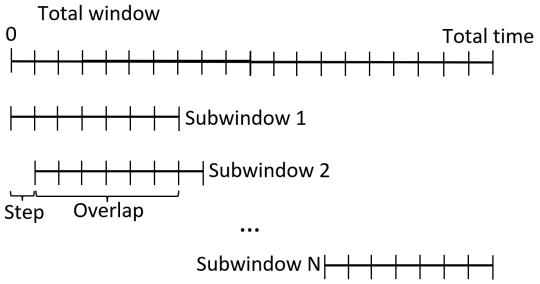

Figure 2.4: Visualisation of a rolling window structure: The subwindows that iterate over the total window.

2.2.4 Probabilistic power spectral density

The probabilistic power spectral density (PPSD) can be described as a combination of the spectrogram and the probabilistic density function [13]. Essentially, it shows the variations in the spectrum, through a histogram of several spectrograms, describing the proportion of time, or probability, that each combination of frequency and SPL occurs.

Figure 2.5 shows an example of an PPSD, with frequency on the x-axis, sound level on the y-axis and time proportion or probability on the color bar. As seen in the PPSD, the sound level, when considering a certain frequency, varies over time. For each frequency, the values are normalized, adding to 100 % over all sound levels. As seen in the figure, which is applied over a long time period of recordings obtained by sensor 1, there is a pattern of common sound levels in each frequency, and the variation in frequency and percentage of time is seen. Further analysis of what exactly is seen will be revisited in Section 4.

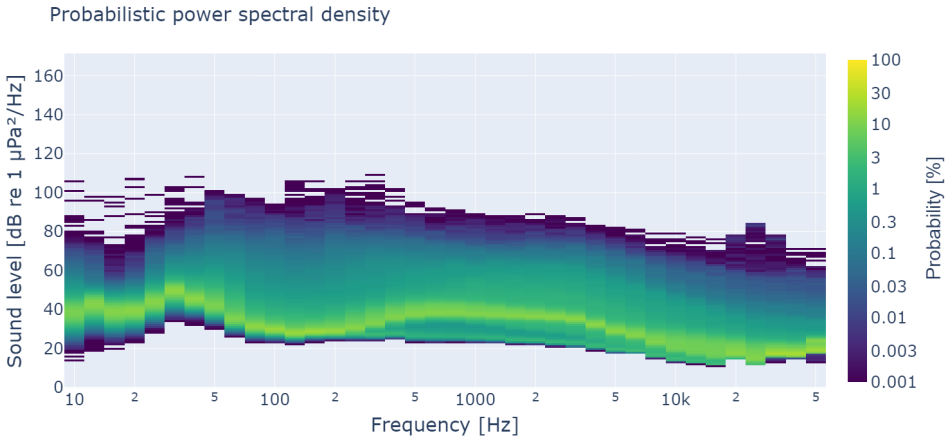

Figure 2.5: A probabilistic power spectral density applied to a large time period for sensor 1.

In this way, the PPSD visualizes both the variations and common sounds or noise of a signal, and the application of the PPSD can be adjusted for the purpose. For a PPSD applied over a larger amount of time, this can be viewed as describing the typical background noise at the location, as the percentage of rain should correspond to a larger amount of time, and boats can be assumed to constitute a smaller portion of the time period, compared to in a small time window including boat passages.

2.3 The basis of the methods to distinguishing boat noise

The approach available to distinguish the noise from other noise is already hinted in the specification of the characteristic noise in Section 2.1.2. The alternatives of concept for the detection methods are energy detection, detecting tones, series of tones or to remove the background noise. Here, the basis of each methods used will be given, in addition to stationarity which is a desirable property in some methods or can impact method choices. Before any analysis is conducted, potential bias in the sound pressure data should be handled by subtracting the mean pressure from the pressure.

2.3.1 Weakly stationarity and equality test

A commonly coveted feature in time series is stationarity, as it affects the performance of several methods. Stationarity is a metric that describes the similarity of statistics in data over time. Strict stationarity is a strong requirement, and regarding measured data, wide sense stationarity is usually "good enough".

Strict stationarity implies that the mean value of the data in a sliding window is zero and that the autocovariance is constant, meaning that the covariance between

the original signal and lagged signal is constant. Meanwhile, wide sense stationarity is when the mean function is zero and autocovariance function is time-invariant. One way to check the stationarity of the measurements is to check the mean and the Pearson correlation function.

The Pearson correlation function is a normalized covariance measurement that results in a value between -1 and 1, consisting of a series of Pearson correlation coefficients. The autocorrelation function is obtained through one time series and a lagged version of the same series. Each lag corresponds to a Pearson correlation coefficient, which is defined as

$$r_{xy} = \frac{\sum_{i=1}^{n}(x(i) - \overline{x})(y(i) - \overline{y})}{\sqrt{\sum_{i=1}^{n}(x(i) - \overline{x})^2}\sqrt{\sum_{i=1}^{n}(y(i) - \overline{y})^2}}, \tag{2.4}$$

where n is the sample size, $x(i)$ and $y(i)$ are sample points and $\overline{x}$ and $\overline{y}$ is the mean of the $x(i)$, respectively the $y(i)$, samples. The ith sample corresponds to $x(i)$ and $y(i-k)$ when the lag is k, see Figure 2.6.

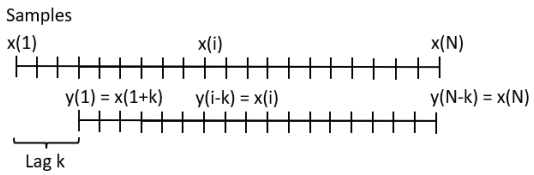

Figure 2.6: The structure of the samples and lags.

When checking the stationarity in a series, the mean and auto-covariance functions are applied in a subwindow with a certain size. Then, it is controlled how many subwindows, or how long time, the statistical features are "similar enough" to be considered stationary. For example, in Figure 2.7 the Pearson correlations of subwindows 0, 1, 2 and 3 are relatively similar to each other, while the correlations for subwindow 50 which is 10 seconds from subwindow 0, are not that similar to the other. Further, a time series can be stationary over a certain time interval in regards to one size of subwindows, but not stationary over the same time interval in regards to another size. A small subwindow tends to include noise in the covariance function, while a large subwindow results in a lower resolution of the statistics.

One way to determine if the statistical features are "similar enough" is through the use of an equality test described by Lund et al [14]. Although some tests compare whether covariances are similar enough, this equality test controls if the *statistics* of the covariances are similar enough [14]. In addition, this test is often substantially more powerful than other tests [15].

The equality test in question is a likelihood ratio test comparing the auto-covariance series in the frequency domain for two subwindows at a time. The fundamental idea of the test is that if the autocovariances of two data series are Gaussian and equal, then the Fourier transformed covariance functions are independent at each frequency and exponentially distributed with the same mean. That is, for two

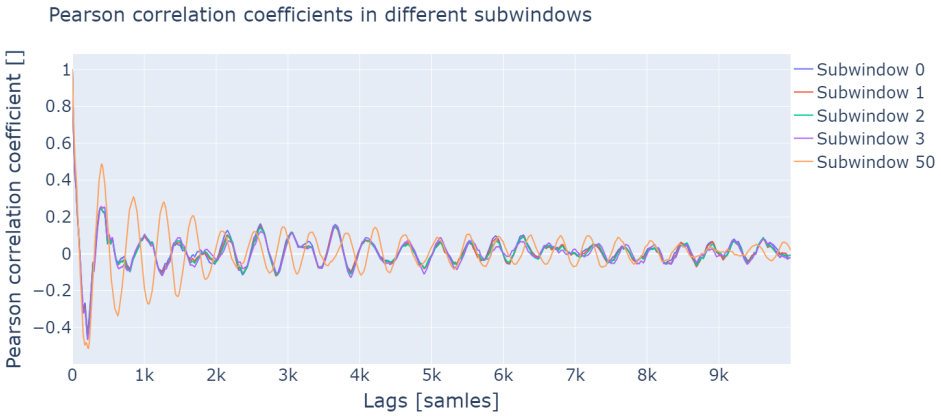

Figure 2.7: Some examples of Pearson correlation coefficients of the sound pressure during a boat passage to demonstrate that the correlation could be very similar over a time of some subwindows, but not similar over subwindows with a larger time distance.

Gaussian independent series X_t and Y_t, $\hat{f}_X(\omega_l)$ and $\hat{f}_Y(\omega_l)$ are independent and approximately exponentially distributed with the same mean $f_X(\omega_l) = f_Y(\omega_l)$, where ω is the angular frequency; $\omega = 2\pi f$. The covariance of the signal is related to the PSD, and applying the Fourier transform to a covariance of the signal gives the PSD. An alternative way to calculate the PSD is through the squared magnitude of the Fourier of the signal [16].

From the basis above, the likelihood ratio, L_{rat}, is defined

$$L_{rat} = \sum_{l=1}^{n/2-1} \ln\left(\frac{4\hat{f}_X(\omega_l)\hat{f}_Y(\omega_l)}{(\hat{f}_X(\omega_l) + \hat{f}_Y(\omega_l))^2}\right), \tag{2.5}$$

where n is an even integer and $\hat{f}_X(\omega_l)$ is the spectral density of the covariance series of the signal subpart X, defined by

$$\hat{f}_X(\omega) = \frac{1}{2\pi n}\left|\sum_{t=1}^{n} X_t e^{-it\omega}\right|^2, \tag{2.6}$$

with $\omega\epsilon[0, 2\pi)$.

If L_{rat} is too small, the equal covariances should be rejected [14]. The condition of the likelihood ratio between two equal covariances, for a large number of samples, and for Gaussian distributed auto-covariances, is

$$L_{rat} < \left(\frac{n}{2} - 1\right)\left[\mu - z_\alpha\sqrt{\frac{\sigma^2}{n/2-1}}\right],$$

where z_α is the z-score of the L_{rat}, or the number of standard deviations between the L_{rat} and μ. It is defined as: $z_\alpha = (L_{rat} - \mu)/\sigma$. The variables μ and σ^2 are the mean and variance in the expected distribution,

$$\ln\left(\frac{4E_1E_2}{(E_1+E_2)^2}\right) \tag{2.7}$$

where E_1 and E_2 are independent unit mean exponential random variates. I.e. the logarithm in (2.7) have the same mean and variance that we expect L_{rat} for many samples to have. To determine μ and σ^2 the distribution in (2.7) is simulated with mean 0 and variance 1 for the exponential random variates. The mean and variance are thus calculated as -0.614 and 0.759 [14].

If the data are not stationary, a threshold could be derived empirically from the data. Another approach is to set an empirical threshold using a graphical method or based on the L_{rat} values.

A previous study using the Kolmogorov-Smirnov test of two samples to investigate stationarity in the ocean has found that time frames of about 430 000 samples, with a sample rate of 441 kHz, are stationary [17]. That is, the ocean recordings were stationary during approximately 0.97 seconds.

2.3.2 Energy detector

One way to try to capture the times when boats are present is to consider the energy levels of the noise. A time signal can be regarded as consisting only of noise, or noise in addition to some added noise, such as background noise and additional boat noise. Thus the signal could be expressed:

$$x_k = \begin{cases} b_k + s_k, & \text{if a boat is present} \\ b_k, & \text{otherwise} \end{cases}$$

where b_k is the background noise and s_k is the emitted noise from boats in the measurement indexed k, meaning that the energy in the signal would reasonably be larger when boats are being present, since the signals should be uncorrelated.

The energy detector is a common and widely applicable detection method used for time series, due to its low implementation and computational complexity and the independence of prior knowledge of the signal. The detector can be applied both on the time and frequency domain, and thus applied to specific bandwidths. As seen above, Parserval's formula implies that the energy in the time domain is equivalent to the energy over all frequencies in the frequency domain.

The energy detector is based on short rolling windows, where the energy, i.e. either of the sums in (2.2) or (2.3), of each subwindow is calculated and compared to a threshold value. If the energy level is above the threshold, the value at that time is set to 1, otherwise to 0, indicating additional noise or boat noise. The energy is calculated as the mean of the squared values within the window, i.e.

$$E = \frac{1}{N}\sum_{k=0}^{N-1} x_k^2, \tag{2.8}$$

where N is the length of the sliding window [18].

In this basic detection version, the parameters to adjust are few, the width of the subwindows and the threshold value. While the simplicity of the detector is an advantage, inflexibility is a disadvantage, as it means that the quality of the detector is dependent on the somewhat stationarity of the process for a threshold to be suitable over time. If the background noise is stationary, and for example follows a Gaussian white noise process $\mathcal{N}(0, \sigma_b^2)$, and the boat noise have an average energy per sample of σ_s^2, then the energy for a large number of samples will approximately follow the Gaussian distribution:

$$E \sim \begin{cases} \mathcal{N}(N\sigma_b^2, 2N\sigma_b^4) \\ \mathcal{N}\left(N(\sigma_b^2 + \sigma_s^2), 2N(\sigma_b^2 + \sigma_s^2)^2\right), \end{cases}$$

and it will be clear when the signal contains the additional noise and not. However, if those conditions do not occur, the performance of the detector will decrease significantly [18]. Though, one can elaborate the energy detector to try to better compensate for the varying and non-white background noise, which will be elaborated further in Chapter 3.

2.3.3 ESPRIT

Another way of detecting boat noise would be to detect the tones that are a distinctive feature of the noise. Tone detection can be performed in several ways. Whether exploiting the attributes of tones or attributes of the noise for the tonal detections, and which method to choose depends on the signal-to-noise ratio (SNR) and the stationarity or nonstationarity of the data.

Estimation of signal parameters via rotational invariance techniques (ESPRIT) is one algorithm that finds the tonal components in a signal and that is offering a higher resolution than the FFT. The ESPRIT algorithm assumes that the measured signal $y_m(t)$ consists of K number of sinusoids and some noise, and estimates the sinusoidal components $x_k(t)$ in

$$y_m(t) = \sum_{k=1}^{K} a_m(\omega_k) x_k(t) + n_m(t), \tag{2.9}$$

where the number of inputs K is known, and where $x_k(t)$ denotes the tones, $n_m(t)$ is the noise at time t and m denotes the index of the output signal. It is assumed that $a_m(\omega_k) = e^{-i(m-1)\omega_k}$, implying that the objective is to determine the frequencies ω_k.

The crucial assumptions of the algorithm are (i) that $(a(\omega_k))_{m+1} = e^{-i\omega_k}(a(\omega_k))_m$, and (ii) that the subspace of the signal can be computed from $y_m(t)$. Due to this, it is possible to isolate the signal subspace and calculate the eigenvalues that satisfy (i). Another implication of (ii) is that the algorithm assumes the noise to be Gaussian white noise, which would require a preprocessing of the data.

Assumption (i) follows naturally when we assume that the sampled signal is a sum of sinusoids and noise. The second assumption, (ii), takes some more rows to

show, but will be verified in the following. In short, assumption (ii) follows from the assumed form of the signal described by (2.9). Equation (2.9) on vector form is written

$$\mathbf{y}(t) = \sum_{k=1}^{K} \mathbf{a}(\omega_k) x_k(t) + \mathbf{n}(t),$$

where $\mathbf{a}(\omega_k) = (1\, e^{-i\omega_k}\, e^{-i2\omega_k}\, \dots\, e^{-i(M-1)\omega_k})^T$. Using matrix form and block matrices yields

$$\begin{aligned} Y = AX + N = U\Sigma V^* &= \begin{pmatrix} U_S & U_N \end{pmatrix} \begin{pmatrix} \Sigma_S & 0 & 0 \\ 0 & \Sigma_N & 0 \end{pmatrix} \begin{pmatrix} V_S & V_N & V_0 \end{pmatrix} \\ &= U_S \Sigma_S V_S^* + U_N \Sigma_N V_N^*, \end{aligned} \tag{2.10}$$

where $U\Sigma V^*$ denotes the singular value decomposition, and the operator * denotes the Hermitian transpose. Thus, the singular values in Σ are sorted in descending order, with the corresponding eigenvectors. With a good SNR of the signal the largest eigenvalues of Y should correspond to the sum of sinusoids, and therefore the columns in U_S constitute the signal subspace. That is why the block matrix partitioning into a signal and a noise contribution term above is reasonable. Together with the system model, partitioning implies that $AX = U_S \Sigma_S V_S^*$ and $N = U_N \Sigma_N V_N^*$. Also note that since U_S and V_S are unitary matrices, we can write $U_S = AXV_S\Sigma_S^{-1} = AF$ where F is an invertible matrix. This detail we will get back to.

To calculate the signal subspace, the autocorrelation matrix of Y can be used.

$$R_{yy} = \frac{1}{T} \sum_{t=t_0}^{T} \mathbf{y}(t)\mathbf{y}(t)^* = \frac{1}{T} YY^* = \frac{1}{T} U\Sigma\Sigma^* U^* = \frac{1}{T} U\Sigma' U^*,$$

where T is the last time index. From (2.10) it is evident that R_{yy} can be decomposed as

$$R_{yy} = \frac{1}{T} U_S \Sigma_S' U_S^* + \frac{1}{T} U_N \Sigma_N' U_N^*,$$

when using the SVD and extracting the K first columns.

Continuing toward finding the eigenvalues of the signal components, the matrices $J_1 = (I_{M-1}0)$, $J_2 = (0I_{M-1})$ and $H = diag(e^{-i\omega_1}, e^{-i\omega_2}, \dots, e^{-i\omega_K})$ are introduced. From (i) it follows that

$$J_2 A = J_1 AH.$$

Using the noted fact from above, $U_S = AF$, yields

$$J_2 U_S = J_1 U_S F^{-1} HF.$$

Introducing $S_2 := J_2 U_S$, $S_1 := J_1 U_S$ and $P := F^{-1}HF$, gives $S_2 = S_1 P$, which can be solved with the least-squares method. The eigenvalues of P, λ_k further corresponds to $\alpha_k e^{i\omega_k}$. Thus, the relative amplitude and the frequencies of the found tones can be extracted from the eigenvalues.

Thus, the algorithm summarises to:

1. Collect: $\mathbf{y}(1)$, $\mathbf{y}(2)$, $\mathbf{y}(3)$, ...
2. Estimate K.
3. Compute the auto-covariance matrix. Either from covariance or based on the signal: $R_{yy} = \frac{1}{T}\sum_T \mathbf{y}(t)\mathbf{y}(t)^*$.
4. Compute the SVD of R_{yy}, and extract the signal subspace from U.
5. Compute S_1 and S_2.
6. Solve $S_2 = S_1 P$.
7. Compute the eigenvalues λ_k of P.
8. Extract the phases and absolute values of the eigenvalues to finally obtain the frequencies and relative magnitudes of the signal.

The parameter choices of ESPRIT are crucial for accuracy. The parameters to set are the dimension of the signal, $dim(S + N)$, the length of the time series used and the model order corresponding to the number of sinusoids, K.

Regarding the dimension of the signal, ESPRIT has no upper limitation, but a too high order can significantly decrease the performance of the algorithm. As a reference, the model order in the MUSIC algorithm, the predecessor of ESPRIT, shall follow $dim(S + N) > 2K$ for real signals. Compared to MUSIC, ESPRIT is less computationally heavy.

One way to set K is by testing ESPRIT for different values and then applying the Akaike Information Criterion (AIC) or Minimum Description Length (MDL) which penalize excessive complexity in models [16].

Just as in the case of the FFT, implementation in a larger time window implies a higher frequency resolution and lower time resolution.

Chapter 3

Method

3.1 The data

The data being used was measured sound pressure, radar data of passing boats and weather data collected at Vasholmarna.

3.1.1 The sound measurement

The sound recording was collected continuously during a three-week period in summer in 2023; from June 22 to July 11. The sound was recorded by IVL following the national best practice refined in corporation with FOI and KTH, using seven hydrophones in seven different locations with varying depth between 5 and 19 meters and varying seabed types, see Figure 3.1 and Table 3.1.

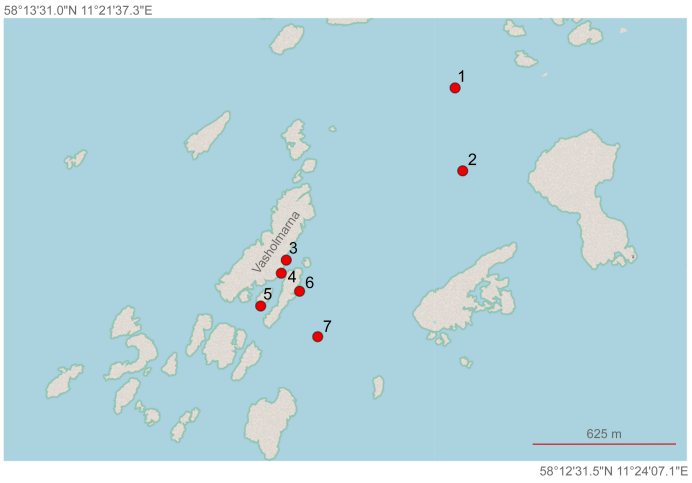

Figure 3.1: The measuring positions at Vasholmarna.

Position	Depth [m]	Seabed type	Logger
1	13-14	Flat bottom, sand	RTSYS
2	15	Flat bottom, sand	RTSYS
3	5-6	Near rock and adjacent to the shore, sand	Soundtrap
4	5-6	Near steep rock and adjacent to the shore, sand	Soundtrap
5	9-10	Near vertical rock and adjacent to the shore	DSG
6	5-6	Near steep rock and adjacent to the shore, bedrock	Soundtrap
7	19	Flat bottom, sand	DSG

Table 3.1: The depth, seabed type and loggers of the recording positions.

As seen in Table 3.1, three different types of loggers were used, RTSYS, Soundtrap and DSG. The Soundtrap hydrophones are shown in Figure 3.2. The sampling frequency used was 128 kHz for the RTSYS loggers and 96 kHz for the others.

Figure 3.2: The three Soundtrap loggers used to measure the underwater noise.

The recorded sound pressure at sensor 1 for a few seconds is shown in Figure 3.3 below. Both the noise from a boat passage and the regular background sound is visible.

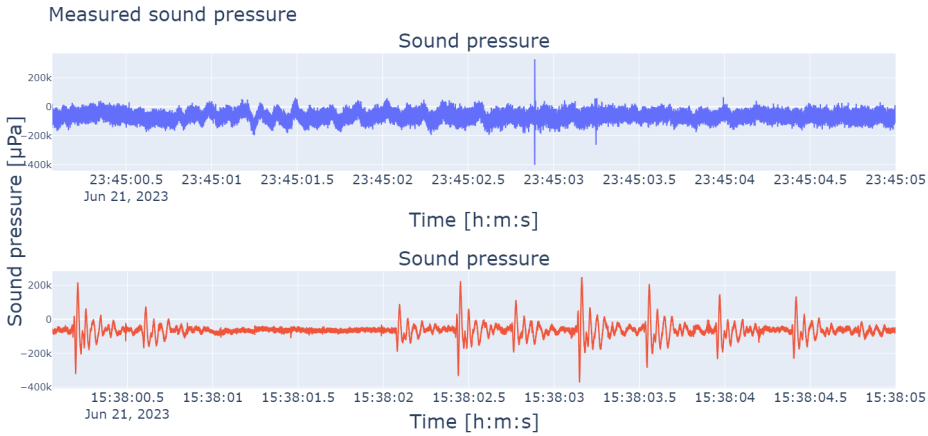

Figure 3.3: The recorded sound pressure at two different times. Data above only including background noise, data below including boat noise.

3.1.2 The weather data

The weather data only included precipitation data during the period of sound recordings, as the noise contribution from wind at the locations was small. It was provided by Göteborgs Universitet, through Kristineberg marine research station, and thus recorded about 5 km away from Vasholmarna.

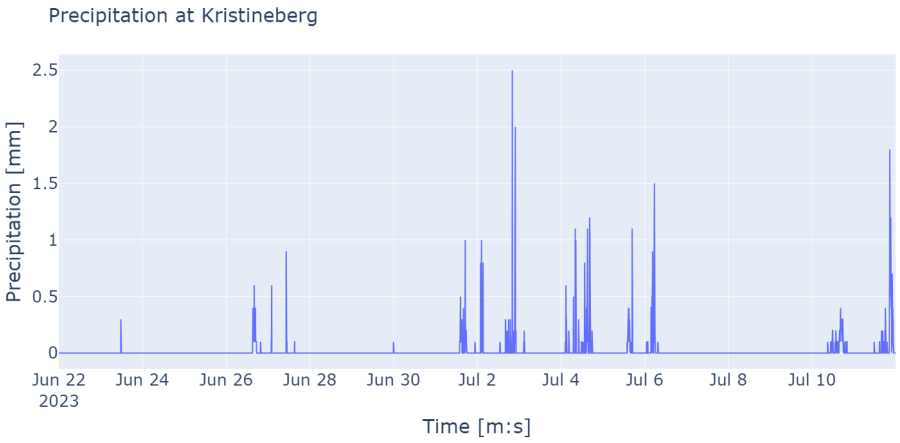

Figure 3.4: The precipitation at Kristineberg during the period of measuring underwater noise.

3.1.3 The radar data

The radar data was recorded between 12.00 and 15.00 on the 11th of July by a marine radar of type Koden. The radar was built to be placed on boats, but was here mounted on a tripod, as shown in Figure 3.5. A GPS compass provides compass directions to the radar so that it could report the position of objects detected. The operator clicked on the radar screen to specify that a boat should be tracked and saved. Hence, some boats were potentially unnoticed, and some passages probably cut short at the end or beginning of the route. Also, the radar sometimes switched from tracking a boat to tracking an island if a boat got close to an island. In addition, software was developed to store detected objects from the radar and to calculate the distance between the boats passing and each sound recording location.

Figure 3.5: The radar used to capture the boat passages.

3.2 Bias, stationarity and the methods

Before investigating stationarity, applying the energy detection method, the PPSD and the ESPRIT method the data were pre-processed by eliminating possible bias caused by a non-zero mean.

Bias removal of a fluctuating bias can be done very accurately by using a standard moving average or computing the mean in a rolling window, moving one sample at a time. Due to the computational heaviness and adequate accuracy, the removal of bias was done by moving average without overlap. When setting the subwindow size, two factors were specially considered; the noise in the samples and potential variations in the bias.

3.2.1 Wide sense stationarity

Wide sense stationarity was verified by using the mean and Pearson correlation coefficient in a rolling window structure. By testing several subwindow sizes, a subwindow size of 1.6 seconds was considered suitable with a step size of 0.2 due to

the computational heaviness, and the step size is still not too large for stationarity over the subwindows to be found.

In each subwindow the mean was calculated and the Pearson correlation coefficient described by (2.4) for lags up to 10 000 was calculated. This, to avoid unnecessary computational heaviness as the trend would continue after 10 000 lags, or $10000/f_s = 0.078$ seconds, while the correlation coefficient would become less reliable as fewer samples were considered in the coefficient.

To determine how long the statistical features in the data remained constant, the Pearson series were compared using the equality test described in Section 2.3.1. This was done by choosing the signal subpart of a reference subwindow X, extracting the covariance series, and iterating over the covariance series of the following subwindows, calculating the L_{rat} values for X and each of the other subwindow using (2.5), and further the obtained L_{rat} were compared to the limit. The limit was calculated through estimated μ and σ^2 to correspond to the exact distribution of the PSD. The estimations were obtained by 180 calculations of (2.7), one for each subwindow, using the PSD, or the Fourier transformed Pearson correlations of the subwindows, instead of the simulations E_1 and E_2. The estimations of μ and σ^2 were the mean, respectively, standard deviations of the 180 calculated values.

The stationarity test was only applied to sensor 1, both in times of nonprecipitation with no boats and with a boat present. To get a good representation of the stationarity results, the test was performed using the covariance of several of the subwindows, or X, as a reference to compare the other subwindow, Y, to. Initially, the first subwindow would be used as the reference subwindow, X. In the following, X was chosen as the subwindow corresponding to the largest change in the series of L_{rat} values.

3.2.2 Probabilistic power spectral density

To get an general understanding of the variations in the soundscape at different locations of the sensors, and to obtain a clearer picture of the variation due to boats, the PPSD was calculated over different time intervals. It was calculated both for some long periods spanning days and over shorter time intervals of three hours. Long PPSDs were used to compare the background noise at different locations, and two short PPSDs for each sensors were used to quantify the noise contributions. One PPSD during the quiet night data and one during the boat passages during the day, as much as possible avoiding precipitation. For information on the exact data used in the PPSDs, see tables 3.2 and 3.3.

The fundamental form of a PPSD has, as mentioned, similarities to a histogram and is achieved through the utilization of a rolling window iterating over a time period and calculating a spectrogram in each subwindow. The spectrograms are then used to eventually determine how usual each combination of frequency and sound level is seen to all subwindows. The size of the subwindow and the step size of the rolling window were 10 seconds. The spectrograms were calculated through rolling windows with subwindows and a step size of 1 second, and with a Hann window applied.

In addition, the frequency bins of the PPSD were determined to be the logarithmic intervals of the frequency range in each spectrogram, and the resolution of the sound level was established. The histogram was obtained by calculating the number of appearances in each sound level bin, considering one frequency at a time. A normalization of the probability axis was desired so that all possible outcomes/noise levels for a noise of a certain frequency correspond to 1. That is, the total probability is equal to 1 when all noise levels in each frequency are summed, independent of the resolution of the frequency windows. Due to normalization, the probability dimension was given in percentage per dB. Also, the probability axis was logarithmized so that the variation of small probabilities would be visible in the PPSD.

Table 3.2: The time interval and duration for the application of the long PPSD.

Sensor	**Start time [day, time]**	**End time [day, time]**	**Duration [days]**
1	23/6, 00.00	24/6, 19.00	2
2	22/6, 01.00	24/6, 11.00	2.5
3	22/6, 14.00	30/6, 00.00	7.5
4	22/6, 14.00	11/7, 17.00	19
5	22/6, 14.00	9/7, 08.00	16.5
6	22/6, 14.00	11/7, 10.00	19
7	22/6, 14.00	2/7, 06.00	10

Table 3.3: The start times of the PPSD applied on time with boat passages and in night time to see the noise contribution.

Sensor	**Start time of the boat PPSD [day, time]**	**Start time of night PPSD [day, time]**
1	22/6, 10.00	23/6, 01.00
2	22/6, 08.00	23/6, 01.00
3	24/6, 15.00	23/6, 04.00
4	8/7, 11.00	23/6, 04.00
5	24/6, 15.00	23/6, 04.00
6	9/7, 13.00	22/6, 02.00
7	11/7, 09.00	22/6, 02.00

3.2.3 The energy detector

The energy detector used to try to find boat noise was an elaboration of the basic version explained in Section 2.3.2. This detection method can be described as two energy detectors with different time intervals that move equally fast, as shown in

Figure 3.6. The short subwindow is for detection of temporarily high energy levels, and one longer as an approximate of the background energy level, allowing one to include weather influences.

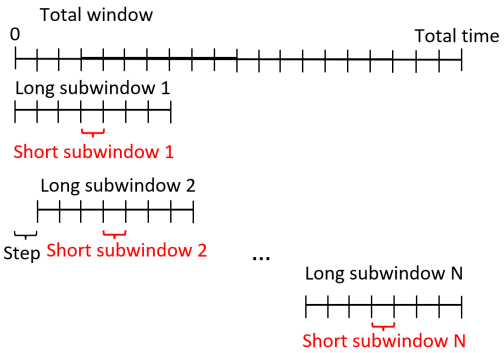

Figure 3.6: Visualisation of the construction of the energy detection method with two combined rolling windows.

The practical implementation of this detector was only one rolling window with a long subwindow of 10 minutes, from which a short middle part was extracted as the short subwindow. The time frame of 10 minutes seemed to capture background noise and temporary rain. To find a suitable size of the short window, balancing the resulting noise and the usually minute long boat passages, windows of different size were tested. The detector was applied to the data from 12.00 to 15.00 on the 11th of July when a radar measured the distance to present boats. The detector was also applied at times when raining at the location of each sensor to see possible change in performance. The precipitation showed to vary locally in the area and therefore the time period for each sensor differed. The precipitation data were a guidance to finding measurements including rain noise.

In each of the subwindows the bias was removed using a suitable window size, and the energy calculated by (2.8) in the long and short subwindow. In addition, the energies were converted to dB levels by (2.1). The temporary energy level and the approximated background energy level in each short, respectively, long subwindow were divided or, in practice, subtracted since the energy were given in dB. This was done to obtain a measure of the energy taking the background noise into account.

To determine whether the energy included noise from a boat, the final energy levels were compared to a threshold of 5 dB, as it seemed reasonable seen to the data.

As a verification of the detector, the times of boat passages were also noted. The time stamps of the passages indicated the time in minute precision when the boats were closest to each sensor, based on the radar data. To determine the number of false negative, true and false positive boat flags, flags within 2 minutes of the time of a boat were allowed. The detector was applied to all sensors during the time of the radar measuring, except for sensor 6 which was retrieved from the water earlier.

3.2.4 ESPRIT method

The method was applied to sensor 1 and the application was carried out in the following way: The bias was removed, the number of sinusoidal components, K, was tested for 2, 5, 10 and 15, to hopefully find the most intense tones, and $dim(S+N)$ was tested for 100 and $2K+2$, following the MUSIC rule of thumb [16]. The length of the signal, which affects the time and frequency resolution, was set to 1 second. The implementation was verified through a simulation described in Appendix A.

Chapter 4

Results

4.1 Bias

The bias in the sound pressure data fluctuated over time. The average plots based short subwindows lasting some seconds or a few minutes were dominated by noise. Already in the 30 second subwindow a trend in the bias was visible in each sensor data. But the average values still look noisy, as seen in Figure 4.1a.

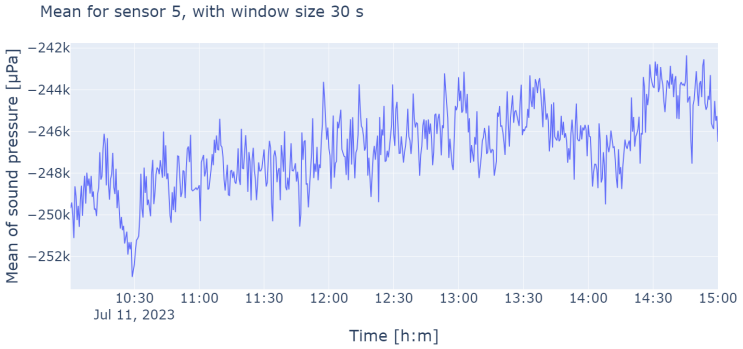

(a) The average sound pressure using 30 second subwindows for sensor 5.

Figure 4.1: The average sound pressure using different subwindow sizes.

With a growing subwindow the average values got less noisy and the trend was clearer, see Figure 4.1. The subwindow of 10 minutes seemed to be suitable for the bias removal, removing the noise without compromising the trend resolution too much.

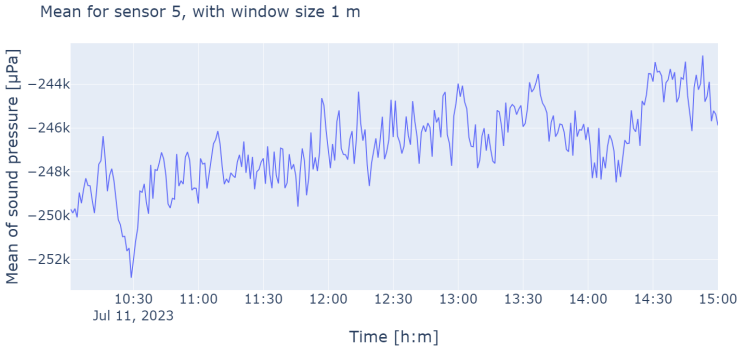

(b) The average sound pressure using 1 minute subwindows for sensor 5.

(c) The average sound pressure using 2 minutes subwindows for sensor 5.

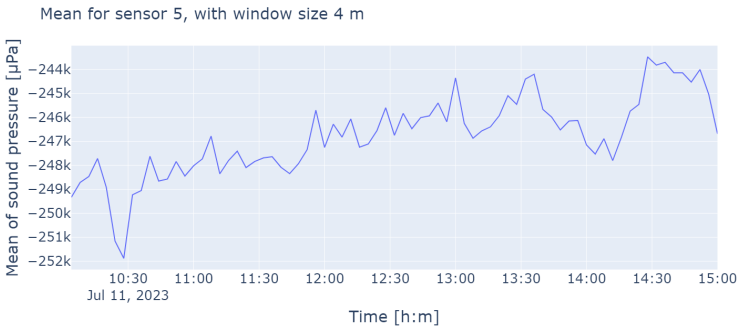

(d) The average sound pressure using 4 minutes subwindows for sensor 5.

Figure 4.1: The average sound pressure using different subwindow sizes.

The data from sensor 5 was noisier then other data, hence the need for extra attention to that sensor when determining the subwindow size. For the average plots of the additional sensors, see Appendix B. In general all sensors had a trend and the trends were different for different sensors. The trends for sensor 1 and 2 which were located closely and in similar surroundings lacked similarities. The

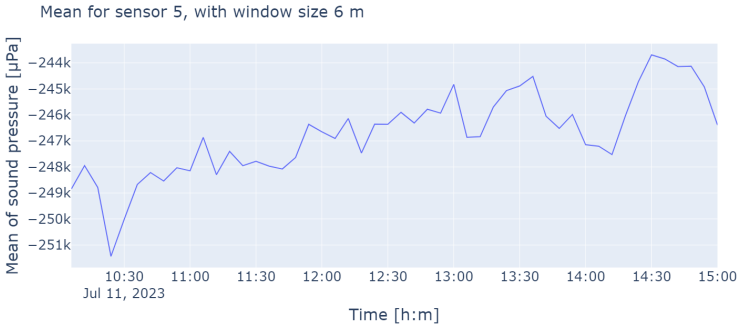

(e) The average sound pressure using 6 minutes subwindows for sensor 5.

(f) The average sound pressure using 10 minutes subwindows for sensor 5.

Figure 4.1: The average sound pressure using different subwindow sizes.

same was true regarding sensor 3, 4 and 7.

4.2 Stationarity

The Fourier transformed Pearson correlation series, i.e. PSDs, for some of the subwindows, whose potential equalness was to be determined, are visible in Figure 4.2 below.

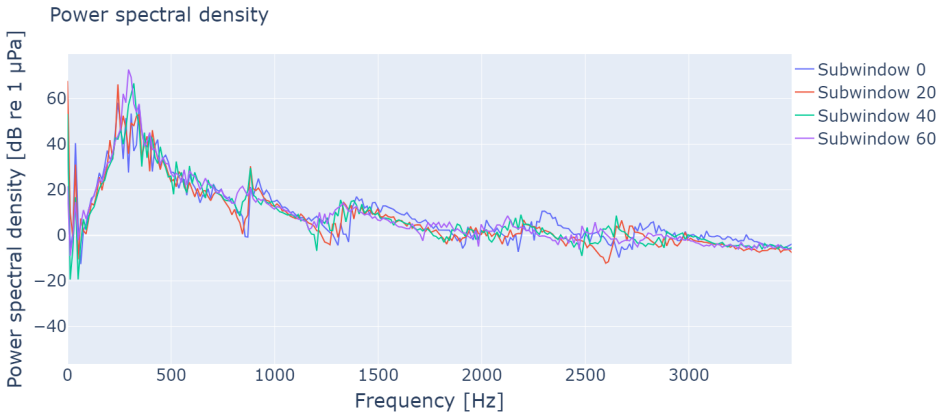

(a) The PSDs for some subwindows during a boat passage.

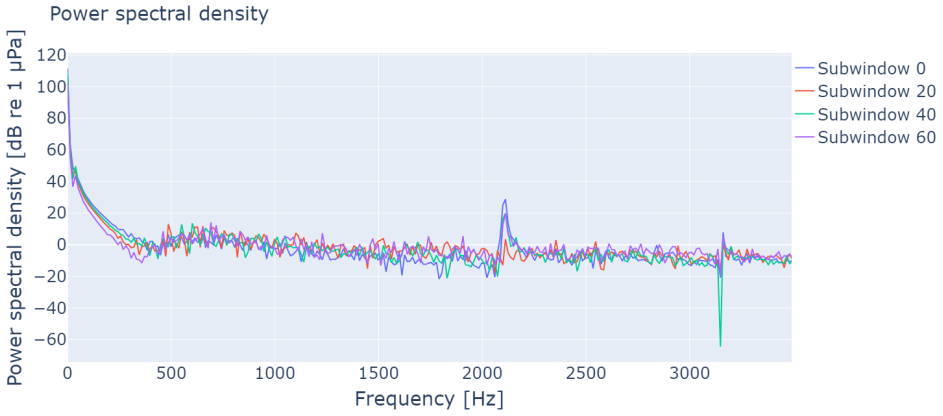

(b) The PSDs for some subwindows during background noise.

Figure 4.2: Some PSDs zoomed in on the lower frequencies.

The empirical results of expression 2.7 for each pair of subwindows, for some Y are showed in figure 4.2. The values in the plot were intended to represent the expected distribution to be able to set suitable values of the estimated μ and σ^2. Only the terms, corresponding to the frequencies in the plot, are used for the estimation, and 80 subwindows were used for the estimation due to the time consumption of the calculations. So, unfortunately the estimations was based on a small number of subwindows, and only subwindows without boat noise. The μ and σ^2 were obtained as the mean of the means of the frequency and the standard deviation as the standard deviation of the standard deviation of the values, so that a somewhat average distribution of the likelihood ratios would be represented.

Figure 4.2: The empirical limit expression, 2.7, for some pair of subwindows without boat noise.

The comparison of the L_{rat} values with the limit, based on the estimated μ and σ^2 values and $z = -84.5$, is seen in Figure 4.3. As seen in the figure, the boat noise is deemed to be wide sense stationary for a time period of $8 \cdot 0.2 = 1.6$ seconds, as the likelihood ratio is smaller than the limit until the 8th subwindow comparison. The background noise, is deemed to be wide sense stationary for a time of $5 \cdot 0.2 = 1$ second. These results seem reliable, but the time periods are large compared to 0.97 seconds, which was the stationarity of a previous study [17]. The estimation of the statistical values, hence also the limit values, are not perfectly representative since the estimation is based on a small amount of subwindows which none includes boat noise as mentioned. Seen to the PSDs, and the likelihood ratios and limits of another subwindow as reference window, X, a period of about 1 seconds seem reasonably generous. In regards of the analysis above, and for convenience a time frame of 1 second seemed suitable to use in methods requiring stationarity.

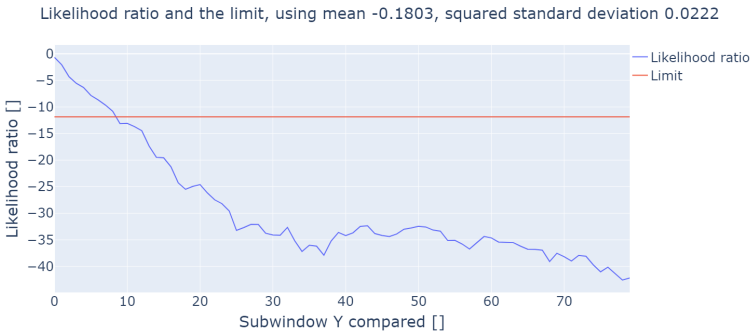

(a) The likelihood values and corresponding limit applied to boat noise.

Figure 4.3: The likelihood values and corresponding limit values, calculated using the estimated μ and σ.

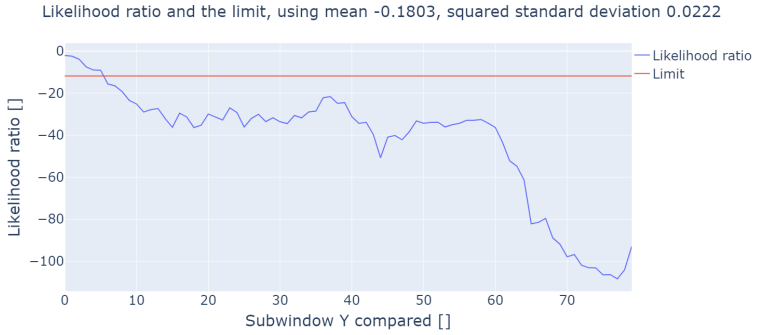

(b) The likelihood values and corresponding limit applied to background noise.

Figure 4.3: The likelihood values and corresponding limit values, calculated using the estimated μ and σ.

4.3 Probabilistic power spectral density

In general the PPSDs applied to long time periods visualized a clear, unique pattern of background noise for each sensor, composed of different sound levels for each frequency range. The comparison of the short PPSDs of different time fragments partly showed the boat noise contribution.

4.3.1 The difference in background noise at different locations

Figure 4.4a shows the PPSD for data recorded at sensor position 1 during a long time frame, see Tabule 3.2. The PPSD shows the probability of different frequency and sound level combinations, with a clear trend. For each frequency range there was a dominating sound level, occurring a large portion of the time seen as the more yellowish green in Figure 4.4a. Similar patterns are visible in the PPSDs for the other sensors as well. This common combinations were assumed to represent the background noise well. The more common noise, or background noise, of sensor 1 is in the range of 20 to 50 dB re $1\,\mu Pa^2/Hz$. When comparing the PPSD for sensor 1 and 2, by comparing Figure 4.4a with Figure 4.4b, the background noise pattern looked similar. For low frequencies, the sound levels at sensor position 2 spanned a wider range than at sensor 1.

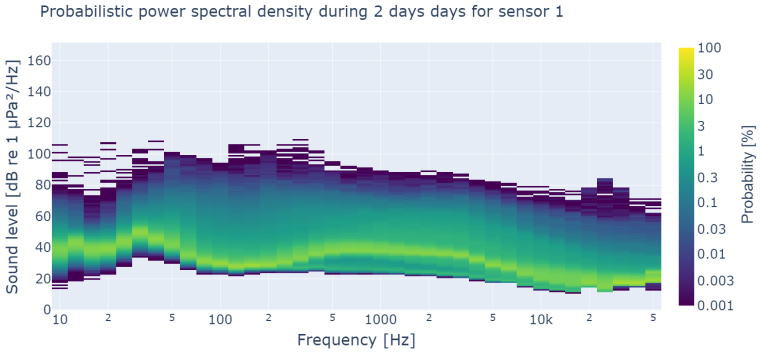

(a) The PPSD during 2 days visualising the background sound at sensor 1.

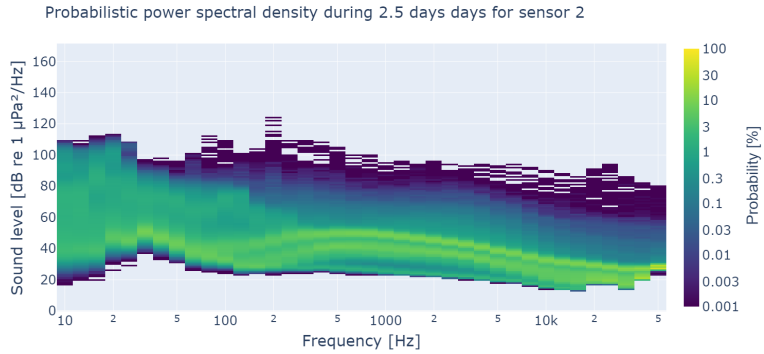

(b) The PPSD during 2.5 days visualising the background sound at sensor 2.

Figure 4.4: The PPSD during a long time period visualising the background sound.

The PPSDs for sensor 3, 4 and 6 showed a background noise with similar pattern of the background noise, as seen in figures 4.4c, 4.4d and 4.4f. The common sound level for these sensors varied around 35 to 70 dB re 1 µPa^2/Hz. The dip in sound level around 30 kHz for sensor 1 and 2 did not appear for the rest of the sensors. Instead there was a dip at 50 kHz for these PPSDs.

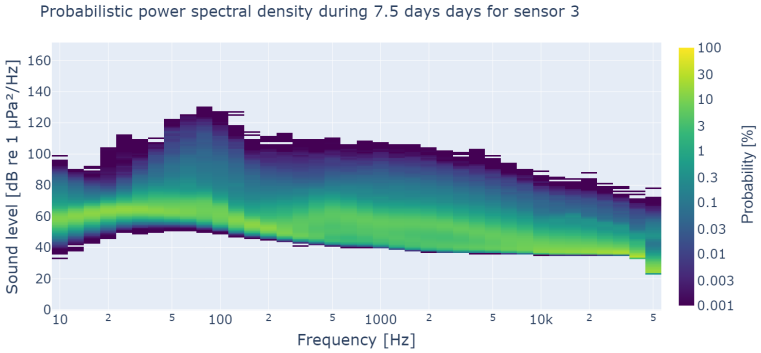

(c) The PPSD during 7.5 days visualising the background sound at sensor 3.

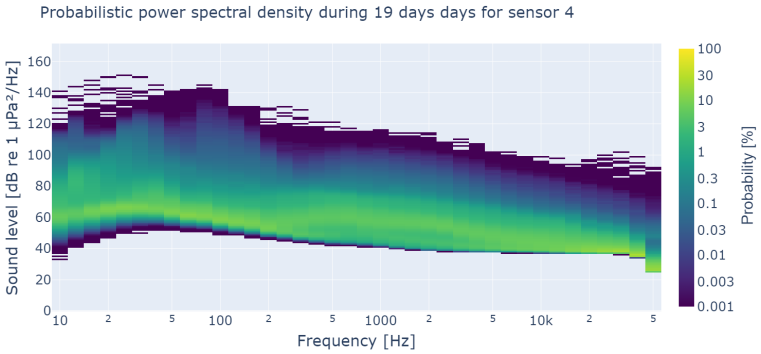

(d) The PPSD during 19 days visualising the background sound at sensor 4.

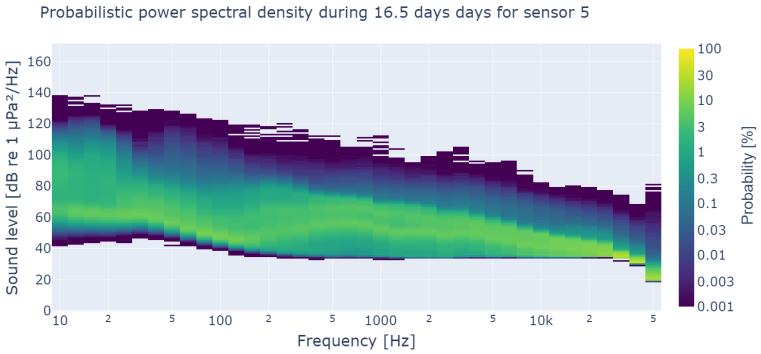

(e) The PPSD during 16.5 days visualising the background sound at sensor 5.

Figure 4.4: The PPSD during a long time period visualising the background sound.

The background noise logged by sensor 5 and 7 are very similar, as shown in figures 4.4e and 4.4g. For both PPSDs the common noise levels of lower frequencies

span a larger range than the background noise for sensor 1, 3, 4 and 6. The maximum common noise level is about 110 dB re 1 µPa^2/Hz. In general the background noise is in the range of about 35 to 80 dB re 1 µPa^2/Hz. Also these PPSD showed a dip in the common sound level at 50 kHz.

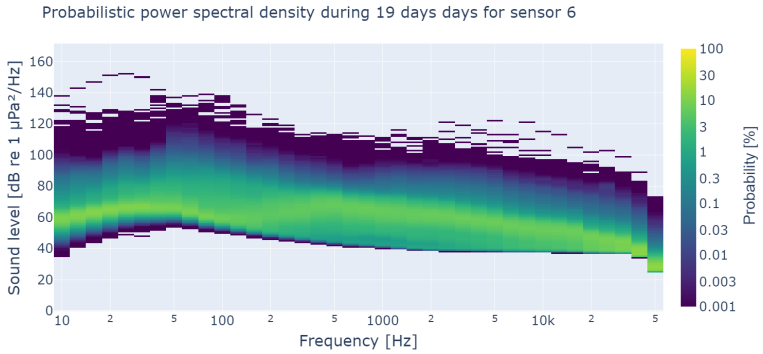

(f) The PPSD during 19 days visualising the background sound at sensor 6.

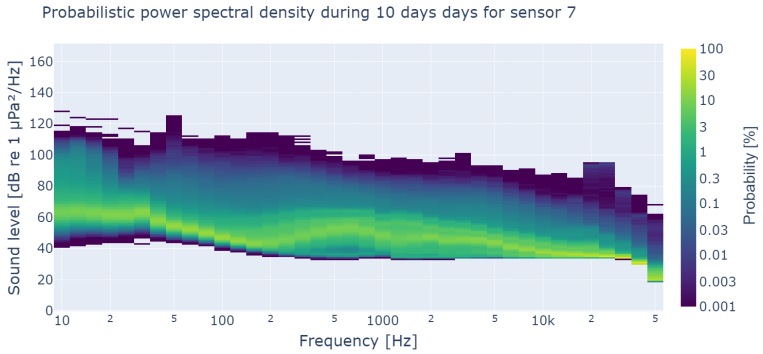

(g) The PPSD during 10 days visualising the background sound at sensor 7.

Figure 4.4: The PPSD during a long time period visualising the background sound.

4.3.2 Comparison to see the boat noise contribution

All PPSDs of the day recordings showed to contain variability and higher noise, for all frequencies but the lowest, compared to the PPSDs of night data without rain which will be seen below. Further, the amount of noise shifted between different sensors.

Especially for sensor 1 and 2, the boat noise was distinct. The PPSD of boat noise shown in Figure 4.5a contained noise that was distinctly more frequent than other noise, apart from the background noise seen in Figure 4.5b. For the corresponding plots of the recordings from sensor 2, see Appendix C. The more frequent noise is seen in the frequencies 1 to 20 kHz. The boat noise, at a maximum reached noise levels of about 60 dB re $1\,\mu Pa^2/Hz$ compared to the background noise at about 50 dB re $1\,\mu Pa^2/Hz$ or 40 dB re $1\,\mu Pa^2/Hz$ during night.

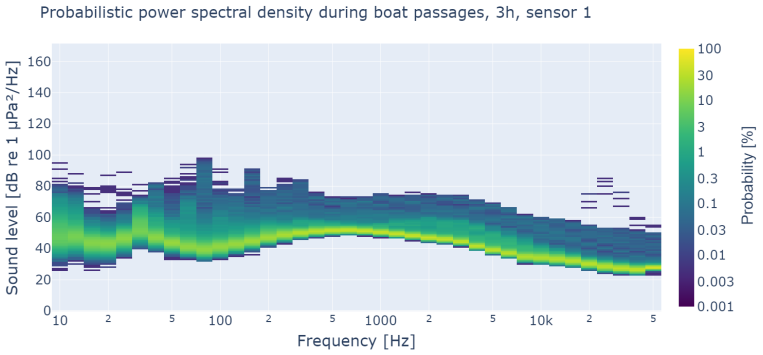

(a) The PPSD during 3 hours containing boat passages for sensor 1.

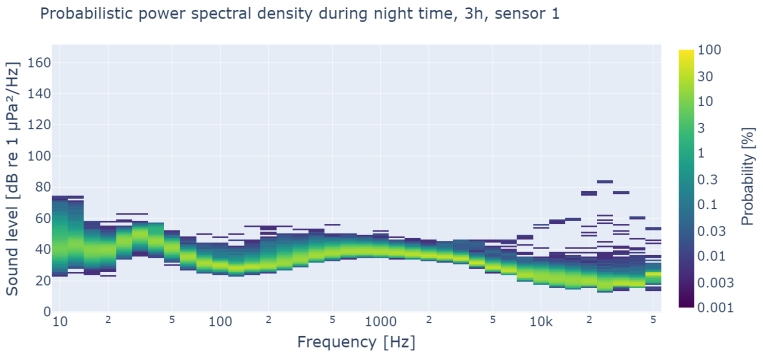

(b) The PPSD during 3 hours in the night for sensor 1.

Figure 4.5: PPSDs during 3 hours, to give a sense of the boat noise contribution.

Comparing the PPSDs of night and boat noise for the other sensors, the added noise is in a large range of frequencies, and the typical level and frequency combination of boats is not as distinct as in previous PPSDs. For the PPSD of sensor 3 in Figure 4.5c, there is a faint but still somewhat more probable area of noise between 1 to 10 kHz reaching 80 dB re $1\,\mu Pa^2/Hz$, which is higher than the background noise. Also at 100 Hz, there was a large increase in the sound levels in the PPSDs including boats. A similar increase was seen in the comparisins of the PPSDs for all sensors.

For sensor 6, there is no such field visible in Figure 4.5e. The sound at all frequencies higher than 200 Hz, cover a broader range of sound levels and the background noise in the PPSD of the boat noise, is not as distinct as in the PPSD of night data, see figure 4.5f.

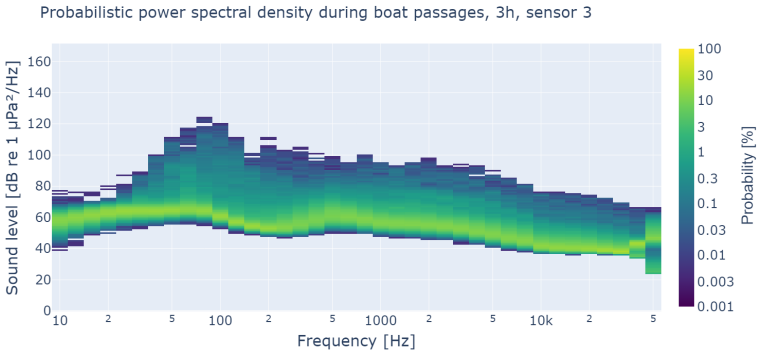

(c) The PPSD during 3 hours containing boat passages for sensor 3.

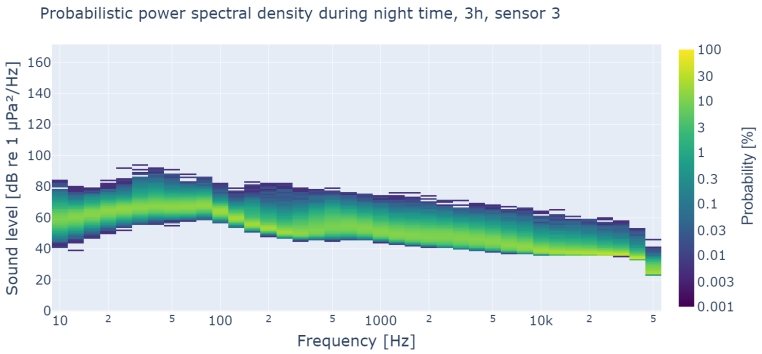

(d) The PPSD during 3 hours in the night for sensor 3.

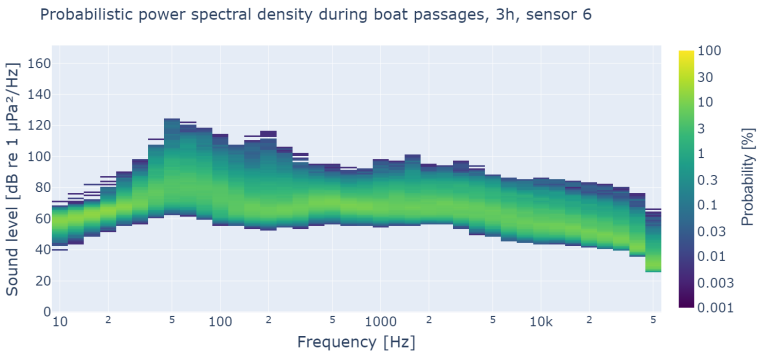

(e) The PPSD during 3 hours containing boat passages for sensor 6.

Figure 4.5: PPSDs during 3 hours, to give a sense of the boat noise contribution.

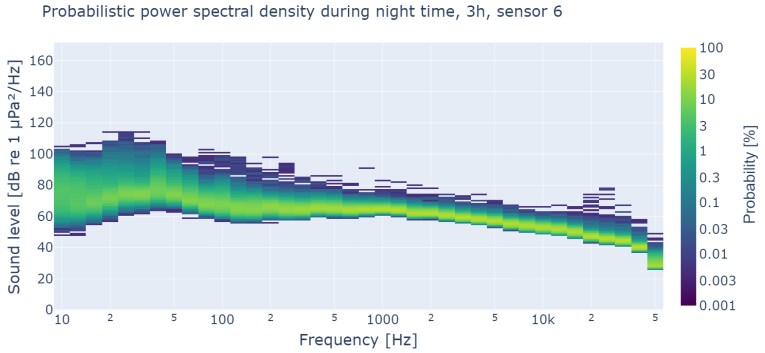

(f) The PPSD during 3 hours in the night for sensor 6.

Figure 4.5: PPSDs during 3 hours, to give a sense of the boat noise contribution.

The comparison of the other sensors, were of a similar result. See Appendix C for the corresponding figures.

4.4 Energy detection

Below the basis of elaboration, and the validation of the detector is presented.

4.4.1 Choice of subwindow size

The resulting energy detector output for different subwindow sizes are visible below. For shorter subwindows some noise was visible, while longer seem to result in slightly too low resolution. Seen to the energy levels in the short subwindow, a subwindow of 20 seconds seemed reasonable both in times of and without precipitation, see figures 4.6 and 4.7. The boats registered by the radar are marked by a dashed line in the energy ratio plots of the time when the radar was used. For some of the times of application of the detector no radar data was available. For comparison of all subwindow sizes see Appendix D.

4.4.2 The resulting detector, partly during rain

The histogram in Figure 4.8 shows the false negative, true and false positive boat flags for each sensor and the mean values. I.e. missed, detected and falsely detected boat passages.

The number of detected boats were highest for sensor 1 and 2. The missed and falsely detected passages were least for the same sensors. Sensor 5 had the highest number of falsely flags, but still missed almost all boats, only a few passages were detected. In general, except for sensor 5, the number of falsely detected boats was low, while the detected passages constitutes approximately 35% of the number of registered boats.

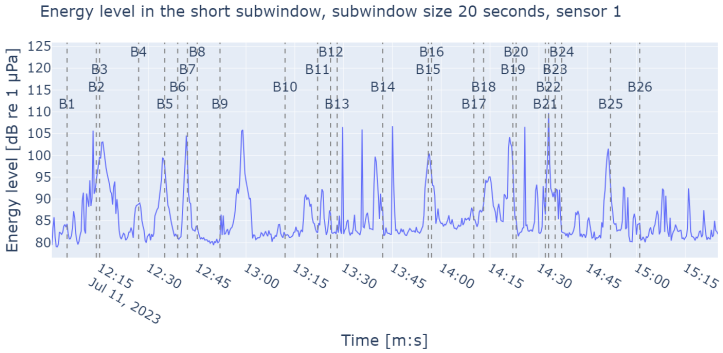

Figure 4.6: The energy level of the short subwindow for subwindow size 20 seconds, sensor 1.

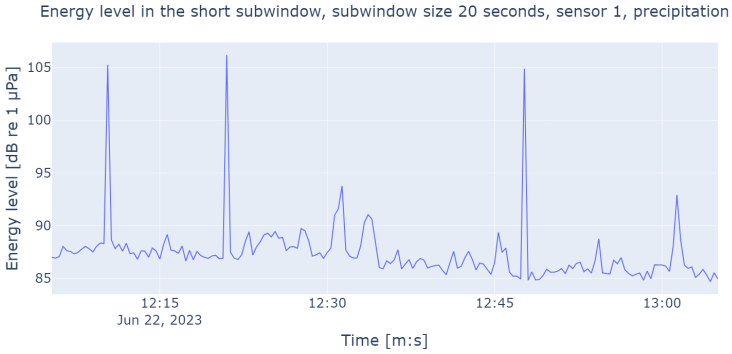

Figure 4.7: The energy level of the short subwindow for subwindow size 20 seconds, sensor 1, during heavy precipitation.

For all sensors the energy ratio level usually fluctuated around 0, with dips and tops. The performance of different sensors varied.

The calculated energy detector output for sensor 1 in Figure 4.9a, shows several clear and distinct energy peaks that coincides well with the radar data. Some energy peaks were smaller than the threshold of 5 dB and not marked as boats, for example at 12:27 and 14:14. At some additional times the energy peaked, but the energy peak was very low. At for example 12:58, 13:38 and 15:15 the peaks were high but no boats were detected by the radar.

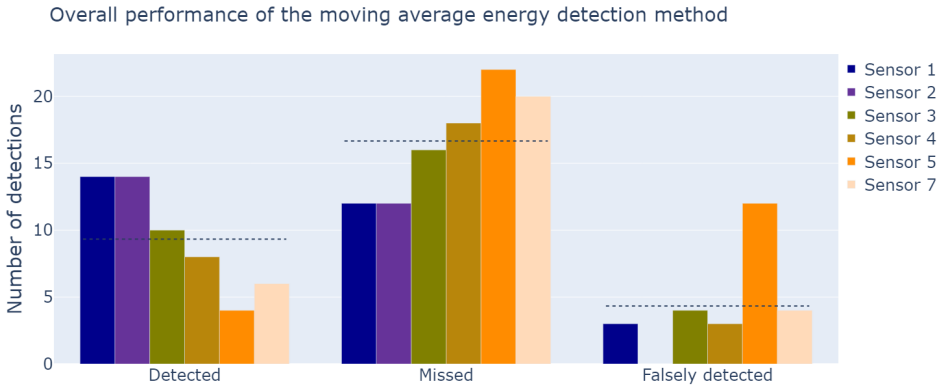

Figure 4.8: The performance of the energy detector in form of detected, falsely detected and missed boats.

The energy detection for sensor 2 in Figure 4.9c was similar to the detection for sensor 1, both in regards to performance and correlation in energy curve. The energy peaks in both plots followed each other pretty accurately. Just as above some energy peaks in the curve were not marked as boats, for example 12:14, 12:30 and 13:00, some of those peaks such as 12.14 were high but surrounded by negative energy dB values and thus not deemed as detected boats.

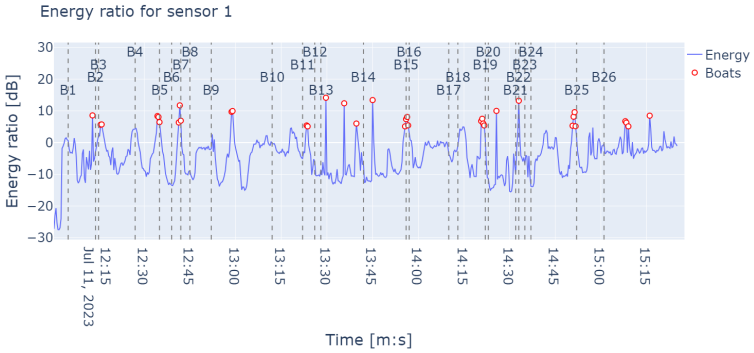

(a) The result of the energy detector for sensor 1.

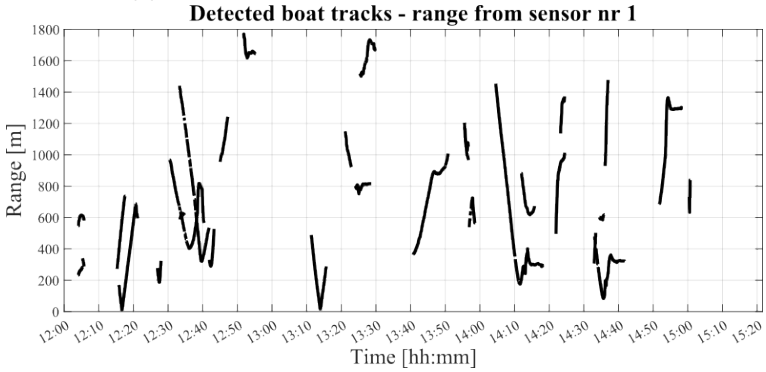

(b) The registered boats and the distance between the boats and the sensor.

Figure 4.9: The energy detection result and the registred boats by the radar.

The energy detector applied to sensor 3 flagged several distinct peaks but also missed many registered boat passages, as shown in Figure 4.9e. At several instances of nonflagged boats, the energy barely gave rise to a peak or a very low peak, for example at 12:01, 12:42 and 13:43. This, despite some of these registered boats were very close to the sensor, as seen in Figure 4.9f. In addition to the detected and missed boats, the general level of the peaks was low. Some peaks, at 14:28 and 14:45 for example were large and broad.

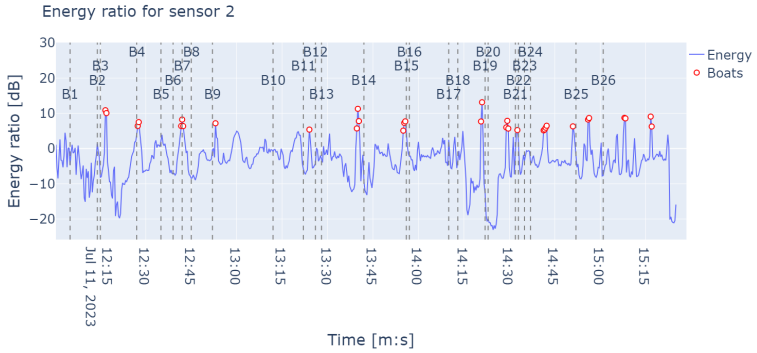

(c) The result of the energy detector for sensor 2.

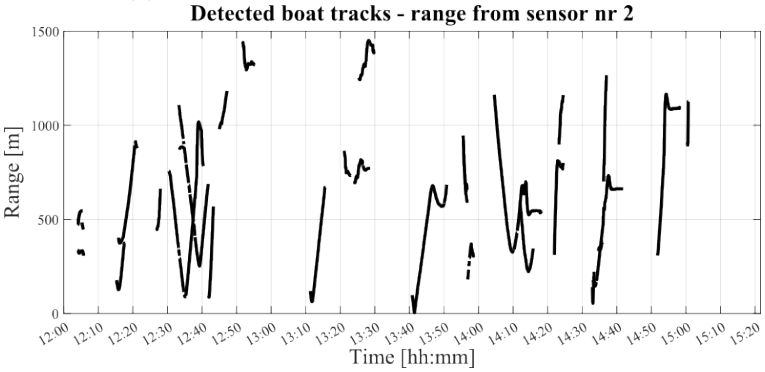

(d) The registered boats and the distance between the boats and the sensor.

Figure 4.9: The energy detection result and the registered boats by the radar.

The energy levels for sensor 4 had similarities to the one for sensor 3, shown in Figure 4.9g. The detector flagged some distinct peaks, but missed most of the registered boats. Often at these times of registered boats there was no peak at all. All boats previous to 12:25 and several between 12:30 and 12:45, were located more than 1 km away. During some of the close registered passages the energy level did not peak at all. Further, some of the distinct energy peaks were not close to registered passages.

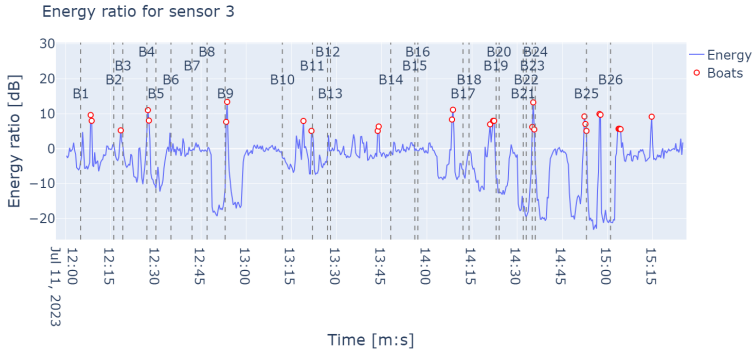

(e) The result of the energy detector for sensor 1.

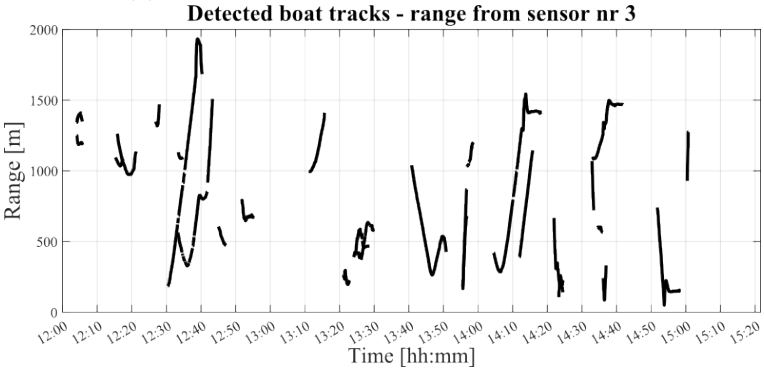

(f) The registered boats and the distance between the boats and the sensor.

Figure 4.9: The energy detection result and the registered boats by the radar.

The data of sensor 5 was, as mentioned, very noisy and that was evident also in the energy levels in Figure 4.9i. Regarding the flagged boats many passages were flagged but many of those times were not within the two minute margin to registered boats. Some of the really close detected boats, about 100 m away, with exceptions at 13.27, were distinctly detected.

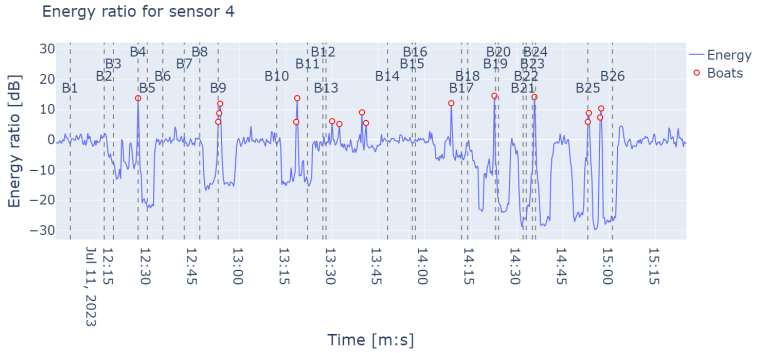

(g) The result of the energy detector for sensor 4.

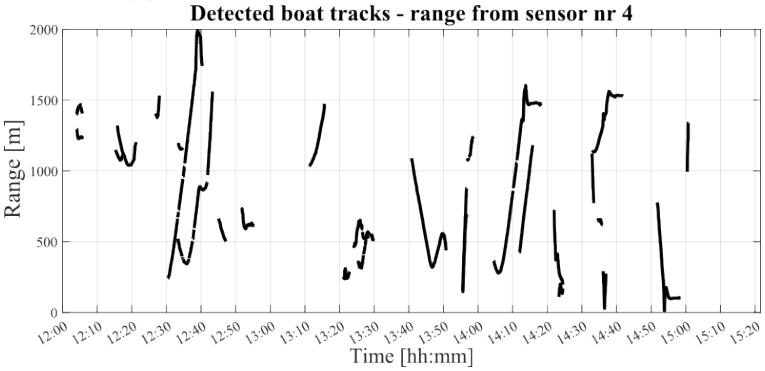

(h) The registered boats and the distance between the boats and the sensor.

Figure 4.9: The energy detection result and the registered boats by the radar.

Also for sensor 7 there were fewer but still distinct boats, as seen in Figure 4.9k. The flags corresponded to boats with varying distance to the sensor. Some of the close registered boats did not correspond to a peak in the energy plot. Further, the energy was more noisy between 12:45 to 13:30 compared to the rest of the plot.

4.4.3 The resulting detector during heavy precipitation

The energy detector was applied as previously stated also to time periods of heavy precipitation to see if the performance shifted. The noise among the energy level ratios differed remarkably between the sensors. For some sensors, the passages of the boats could be clearly distinguished without false detections, as in Figure 4.10a. For other sensors, the energy levels were very noisy and the boat noise and other noise could not be distinguished successfully. Figure 4.10b shows this case with only false detections, which was verified by data spectrograms.

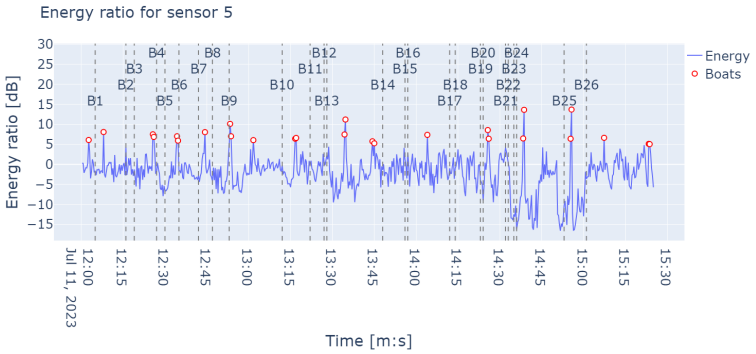

(i) The result of the energy detector for sensor 5.

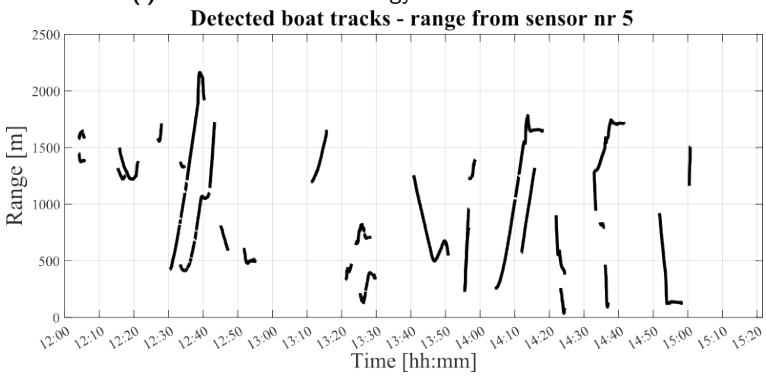

(j) The registered boats and the distance between the boats and the sensor.

Figure 4.9: The energy detection result and the registered boats by the radar.

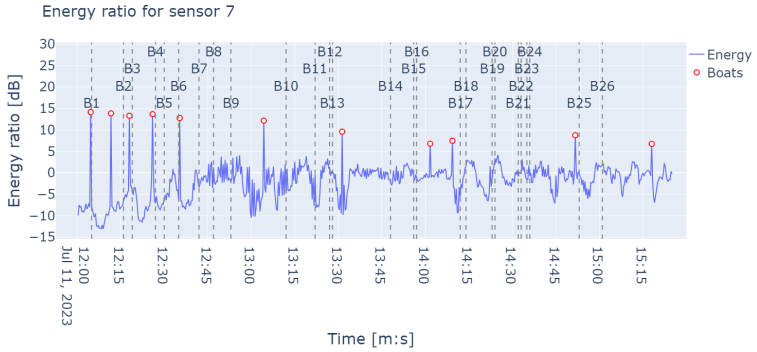

(k) The result of the energy detector for sensor 7.

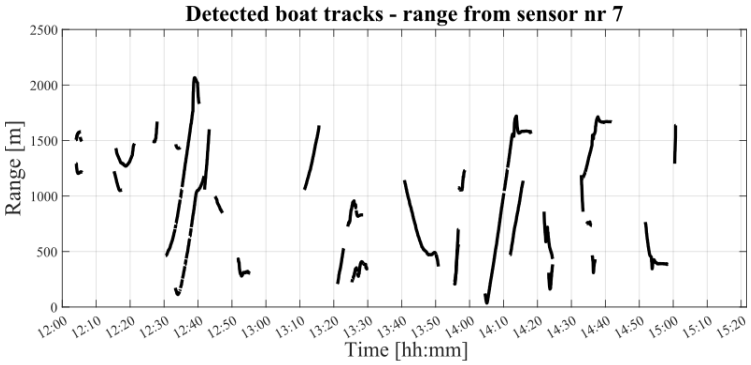

(l) The registered boats and the distance between the boats and the sensor.

Figure 4.9: The energy detection result and the registered boats by the radar.

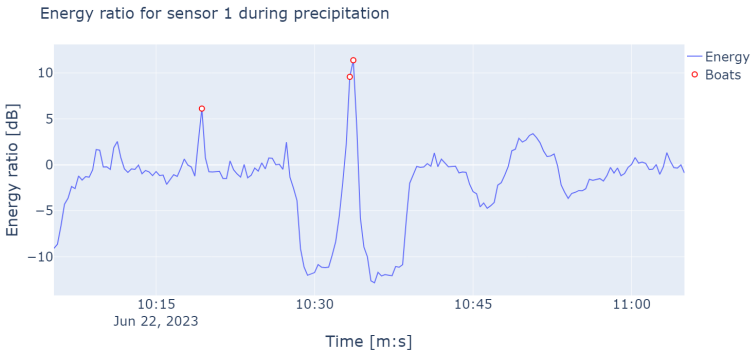

(a) The energy detection result for sensor 1.

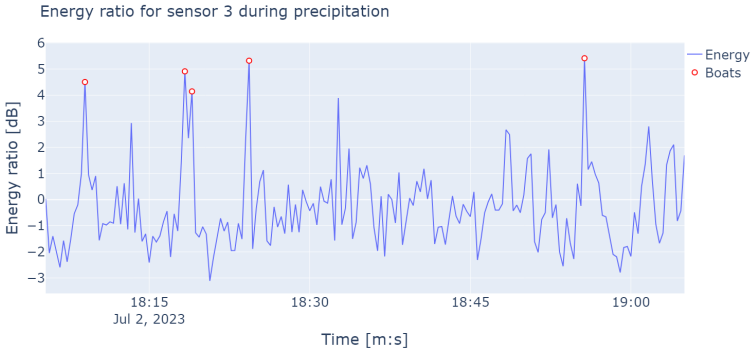

(b) The energy detection result for sensor 3.

Figure 4.10: The energy detection result during a rainy period.

Chapter 5

Discussion

5.1 Overview

Overall, background noise at the different locations was established through the PPSDs. The probable main factors of the similarities in the noise, where seabed geometry and logger type. The energy detector functioned reasonably well for recordings without precipitation, depending on the use of application. Setting a different threshold might adopt the detector for another use and specifying the frequency range might improve the detector. The application of ESPRIT did not work out well, and it was disregarded as a potential detector.

5.2 Bias

Evidently, there was a bias in the data. The fluctuations in the bias possibly depended on differences in the static pressure that were not picked up by the hydrophones. In the plots of the average values, a subwindow of 10 minutes seemed reasonable and was used for the bias removal in the other methods. Of course, the size of the subwindow involves a trade-off between noise and being able to see the structure of the bias, as hinted in Section 3.2.

5.3 Stationarity

The final result of the stationarity analysis was that data have wide sense stationarity for a time frame of 1 second. This result seemed reasonable as observed in the PSD plots, the equality test based on estimated limits, and the reference value of stationarity in the sea of 0.97 seconds from a previous study. The equality test was one alternative among several stationarity tests and was chosen due to its usual solidity.

5.4 Probabilistic power spectral density

The PPSD that spans a long time frame included recordings of varying weather and of nights, and thus a relatively low proportion of boats. Due to this, the statistics contained by the PPSDs in general were considered to be a relatively good representation of the background noise.

The background noise was distinct at all sites and in all frequencies, but the lowest ones. Sensors 1 and 2, sensor 3, 4 and 6, and sensor 5 and 7 showed similarities in background noise, with background noise levels shifting between 20 to 50, 35 to 70 respectively 35 to 80 dB re 1 µPa. A probable cause of these similarities were the positions of the sensors. Sensor 1 and 2 were located close, in a similar depth, and farther away from the islands, probably explains the lower background noise levels. Also, they were of the same sensor type.

Sensor 3, 4 and 6 were located in similarly shallow water. Although sensor 3 and 4 were very closely located and were of logger-type Soundtrap, sensor 6 was farther away, closer to sensor 7. Potentially this is partly due to the high pass filter effect in shallow water, making the background noise at sensor 6 more similar to the others.

Sensor 5 and 7 were placed in very different locations, with different seabeds, depth and structure. The sensors were of the same sensor type, DSG. In addition, weather is a probable contribution of similar recorded noise. The potential effect of the vertical rock at sensor location 5 can not be excluded. In general, one should be careful not to draw strong conclusions out of this. These factors do have an effect on background noise, but the extent should be verified by further investigation.

In all sensors, except for the first two, the sound levels reached a floor. This can be explained by the electrical self-noise of these sensors, making it impossible for those types of sensors to measure levels below about 35 dB.

Furthermore, the dip mentioned in Section 4.3.1 at frequency 50 kHz in sound level seen in all PPSDs except, for sensor 1 and 2 which had a higher sampling frequency, can be explained by the Nyquist frequency of 48 kHz. Since the maximum frequency in the bin was 50 kHz and only frequencies up to 48 kHz were obtained from the signal, the total level of sound in the bin was lower, and thus a lower level of these frequencies was shown even though such low levels could not be recorded by the sensor due to the self noise.

Regarding the noise contribution from the boats, the initial intention was to compare PPSDs of long and short time frames, as the PPSD applied to a short window with the boats would include statistics of a high proportion of the boats. This method turned out to be non-successful. Probably because of the large period of rain in the long windows, making it challenging to distinguish boat and rain noise since these could overlap in frequency and level. Instead, the approach with two short PPSDs described in Section 3.2 was used.

This approach with two PPSDs of short frames has its limitations, but could give

an indication of the boat noise contribution. Especially for sensor 1 and 2 the method was successful in indicating boat noise. At least the distinct noise fields seen there were caused by boats. Whether the boats also caused noise outside the typical frequency and sound levels, we cannot be completely sure without being able to exclude other causes of noise, such as precipitation. This is due to the variation of boat noise both in frequency and sound levels potentially contributing to the probability in other bins. As mentioned, a key for identifying boats is their continuous noise profile, whereas rain has a more irregular noise profile. Since the PPSD does not measure continuous sound, but rather accumulated sound, the rain noise and the boat noise appear virtually the same. Thus, variations in boat noise appear in the same way as rain noise, and there is no evident way of distinguishing them from one another. For example, a long lasting rain and a single subsequent boat passage with overlapping noise seen to frequencies and sound levels can not be distinguished with this method.

The PPSD for sensor 3 also showed a more probable, but faint, field of noise for typical boat noises. For the other sensors, no conclusions about boat noise could be drawn. In addition, sensor 3, 4, and 5 were located in a natural harbor, and the data contained boats idling and moving at low RPM. Additionally, the formation of rocks reflected the noise, and some of the boat noise contribution did probably appear in nontypically high noise levels within their frequency range in those PPSDs.

Consequently, it is crucial that there is no noise contribution caused by precipitation in a PPSD, to be able to draw conclusions about the boat noise. In case of rain, it will only, at most, be possible to get an indication of distinct frequency and sound level combinations of the undoubtedly most common boat noise. Choosing a variation of time intervals or in combination with other analysis tools, it may be possible to draw more conclusions based on the PPSD.

5.5 The energy detector

The choice of subwindow sizes tested was based on the time of a typical boat passage. A short window was desired to prevent broadband rain noise with a semi-high sound level from being mistaken for boat passages. Furthermore, the aim was to detect boat passages even if the windows did not align perfectly with the passages, considering that they typically lasted 2-3 minutes. The choice was also supported by the analysis of broadband noise levels performed by Matzner, who also used 20 second windows [10].

5.5.1 Applying the detection method to the time of radar data capturing

The number of missed, detected and falsely registered boat passages in Figure 4.8 was given in numbers instead of percentage, as there were only 26 observations due to a limited data collection period. Even though more observations are preferred for modeling and more robust testing, it is still possible to draw some conclusions. Further conclusions could likely have been drawn based on controlled measurements, for instance conclusions about the propagation of the boat noise, but it is

very resource-intensive to conduct such measurements over a long period of time. However, before conclusions are drawn, some analysis of what could be observed in the energy level plots is necessary.

Conceptual weaknesses of the detector

As seen the energy dB values usually fluctuated around 0. This is when the values in the long and short subwindows are the same, ideally when there is no additional energy, such as boat noise, in the short subwindow. The negative values appear when the long window goes from excluding to including a lot of boat noise, and the short subwindow thus includes less mean energy than the long subwindow. This complicates the detection of boats that cause an energy peak in an energy dip of negative values, as seen in the plot 4.9c for sensor 2. It potentially also complicates the analysis of the result, since it can be tricky to distinguish if the increase in energy is caused by the phenomena explained, by a boat or any other transient sound source. In the energy plot of some sensors this phenomenon further appears in a series. Whether the energy shifts are caused by the phenomena or by boats can be partly verified on the basis of if the decrease corresponds well to increase of energy levels during the boats, and if the time distance to the boats and negative values correspond to one half of the long subwindow time frame. It can also be verified by looking at the energy level plots in the short subwindows.

Another weakness of the detector concept is that of long boat passages. The detector will not be able to capture boat passages with a high and unison energy level during a time frame longer than the long subwindow. Cases of this, ex long idling, appeared for the sensors located in the natural harbor and was amplified by the reflection in the formation, but were considered acceptable to gain generality of the method.

Difficulties in the performance analysis

The performance analysis of the detector was complicated due to the strict time margin, due to difficulty if several of boats were captured in the same peak, boats not being registered by the radar and boat passages that are far off or with an island in between the boat and the sensor.

The performance analysis of the energy detector was very basic, and a slightly larger margin of time distance between flags and registration would in some cases have led to flags being categorized as detections instead of false detections. Specially in cases where the registered start or end times of passages were off. Perhaps these cases impose a skewness in the results. In addition, some boats were not necessarily registered by the radar, as mentioned in Section 3.1.3. This case was the energy peak at 12:58 seen in most sensor plots. That boat passage was verified on a spectrogram.

Some cases of bad statistical performance of the detector are maybe best explained by the location of the sensor or the boat. In such cases, missed boats should not be a concern, but it require further analysis to know which these occurrences are. Probably some cases for sensor 3 and 4 are such cases, since they are located

between islands and some registered boats are not visible in form of noise in the spectrograms at the times.

The effect of precipitation noise in the data

The inclusion of precipitation noise in the data strongly effect the performance of the energy detector, both causing missed and false detections. Uniformity in the rain is not necessarily challenging for the detector, since it is compensated for by the long subwindow. But because of superposition, the rain partly hides the broad-band component of the boat noise and it takes that the boat noise is very loud for a boat to get detected. This is the case for the missed boats for sensor 7 in Figure 4.9k.

The other challenge related to precipitation is varying precipitation. The difference in noise levels for the sensors is probably due to the variation in uniformity of precipitation. Also, the noisy period in the plot of sensor 7 and the noise in sensor 5 are due to rain.

Improvements of the energy detector

Perhaps the detector applied to periods of varying precipitation could be improved by using a standard deviation-based threshold, since the energy during rain was more noisy. In contrast to a threshold of a certain value, a standard deviation-based threshold would be based on statistics of the energy ratios, and the detector could be configured so that it would only flag energy ratios that are distinctly higher than the noise.

Potentially, the energy detector could also be improved by focusing on the energy within specific frequency ranges. This is enabled by Parserval's theorem, which, as mentioned, enables energy calculation through the Fourier transformed signal. The ranges could then be set to include the typical frequencies of the boat noise. Unfortunately, the frequencies of boat passages partially coincide with the frequencies during rain, so the problem with rain would still not be completely resolved.

It would be good with a precision recall analysis to be able to draw more conclusions about the potential of the method and to be able to set a threshold according to the purpose of the detector. For this precise threshold, the detector may not be good at catching all boats but did flag about half of the passages when it is not raining.

In summary, the detector applied to rainy periods usually decreases the precision but can successfully catch obvious cases of boat noise. During varying rain intensity, the energy is very noisy and the performance is poor since the energy generated from rain and boat passages can then not be distinguished. These cases are somewhat apparent by looking at the curves. Perhaps it could be compensated for by another threshold approach. The alternative approach to limit the frequency range included in the energy would probably not make the detector perfect, but it would improve it significantly.

5.5.2 The ESPRIT method as an alternative

An alternative approach to boat detection is to focus on the tones generated by the engine of the boats. One such algorithm mentioned is ESPRIT. ESPRIT was applied according to the summation of the algorithm in Section 2.3.3, but it was not considered successful for the detection of the boat without the possibility of rigorously testing several combinations of the model parameters, using AIC or MDL. Seen to the frequency, relative amplitude, or pattern of tones, there was no obvious way to determine if a boat caused the tones. The frequency and pattern of tones was very similar no matter if a boat was present; see the Appendix A. In addition, the relative amplitudes of all estimated tones were very high, about 0.97, making it impossible to reject any tones or draw any conclusions based on that.

With more time, it could be worth investigating ESPRIT together with AIC or MDL further, as the tonal components are the strongest characteristics of boat noise. Assuming that boat noise always includes more than one tone, this approach could be successful: ESPRIT finds the most probable frequencies of a signal that is assumed to consist of one or several tones, and AIC/MDL determines the optimal number of tones. So, if the data are found to include only one tone, it could potentially be assumed that there is no boat. Else, the tones could be the fundamental tone and the overtones. However, the parameters of the implementation should be carefully tested, as the simulation showed that the choice of model parameters was decisive.

Potentially the poor result was due to a low SNR and non-filtered background noise, a requirement of the algorithm. This choice was to avoid potential introduction of corruptions in the data, but the intention was to test both versions if the nonfiltered data application would not be successful. If the frequency of the detected tones would have been very low, and thus not caused by boats or rain, the background noise would most definitively have been the cause of the tones. Some low frequency tones were expected, especially since the dominant tones of the background noise were in lower frequencies for sensor 1 4.4a, but that was not the case. Hence, the result could potentially be improved by filtering the background noise, but not certainly. Maybe adjusting the parameters K, $dim(S+N)$ and the application time frame could give rise to results where boat noise can be excluded, but due to time constraints, the approach was bypassed.

Chapter 6

Conclusion

Q1 - To give an overview of how the background noise and boat noise varies in different locations and geomorphological conditions, using spectral statistics:

Using the long PPSDs, an overview of the background noise at the different locations of recordings was obtained. The background noise was seen as the most probable combinations of frequency and noise level, and varied between 20 to 50, 35 to 70 respectively 35 to 80 dB re 1 µPa in the measured frequencies. The geometry of the seabed seems to be one of the main factors affecting the background noise, which seem plausible. Furthermore, the background noise pattern was more similar for sensors of the same logger type.

Using two short PPSDs, the least estimate of the boat noise contribution could be obtained. For sensor 1, 2 and 3 the boat noise was in the range of 1 to 20 Hz and 60, 70 respectively 80 dB re 1 $\mu Pa^2/Hz$ at the specific times of the PPSDs. This method of quantifying boat noise relied heavily on the absence of other sound sources, such as precipitation or biological noise. Using, for example, spectrograms or other additional tools, the conclusions could be strengthened but are still limited for recordings containing rain.

Q2 - To identify boat noise in recorded underwater noise using a energy detector; a signal processing method - and to evaluate the method based on real data, as well as briefly outline alternative conceptual possibilities in detecting boat noise:

The energy detector constructed was a version based on two subwindows, one short and one long to compensate the varying background noise. The resulting energy detector detected about 40 % of the boat passages registered by the detector and the rest were missed. Only a small percentage of the flags were false detections, except for sensor 5, which contained precipitation noise. In general, the detector performed poorer when applying it at times of rain than otherwise. Maybe a different threshold could improve this. In general, a precision-recall analysis would be desired to be able to evaluate the performance of the algorithm more adequately.

The alternatives of concept for boat noise detection are energy detection, tone detection, and detection of series of tones. The detector in this thesis utilized energy levels, but this implied conceptual weaknesses that the other alternatives did not possess, such as compensating energy in the background noise and distinguishing precipitation and boat noise. Thus, the other alternatives could be worth investigating further.

Bibliography

[1] Carlos M. Duarte, Lucille Chapuis, Shaun P. Collin, Daniel P. Costa, Reny P. Devassy, Victor M. Eguiluz, Christine Erbe, Timothy A. C. Gordon, Benjamin S. Halpern, Harry R. Harding, Michelle N. Havlik, Mark Meekan, Nathan D. Merchant, Jennifer L. Miksis-Olds, Miles Parsons, Milica Predragovic, Andrew N. Radford, Craig A. Radford, Stephen D. Simpson, Hans Slabbekoorn, Erica Staaterman, Ilse C. Van Opzeeland, Jana Winderen, Xiangliang Zhang, and Francis Juanes. The soundscape of the anthropocene ocean. *Science*, 371(6529):eaba4658, 2021.

[2] IVL. Miljöpåverkan från fritidsbåtars undervattensbuller. `https://www.ivl.se/vart-erbjudande/forskning/vatten/miljopaverkan-fran-fritidsbatars-undervattensbuller.html`, 2021.

[3] Mikkelsen L. Tougaard J. et al. Hermannsen, L. Recreational vessels without automatic identification system (AIS) dominate anthropogenic noise contributions to a shallow water soundscape. *Scientific Reports*, 9(15477):2045–2322, 2019.

[4] Jennifer Wladichuk, David Hannay, Zizheng Li, Alexander MacGillivray, and Sheila Thornton. Systematic source level measurements of whale watching vessels and other small boats. *The Journal of Ocean Technology*, 14:108–126, 2019.

[5] Alfio Yori. Field study on underwater noise emitted by small tourist boats. comparison between the use of electric and combustion motors. *Archives of Acoustics*, 48:347–358, 08 2023.

[6] School of Physics Sydney. Acoustic impedance, intensity and power. `https://www.animations.physics.unsw.edu.au/jw/sound-impedance-intensity.htm`, 2024.

[7] Robert J Urick. *Sound propagation in the sea*. Peninsula publishing, 1982.

[8] Nienke C.F. van Geel, Denise Risch, and Anja Wittich. A brief overview of current approaches for underwater sound analysis and reporting. *Marine Pollution Bulletin*, 178:113610, 2022.

[9] Gordon M. Wenz. Acoustic Ambient Noise in the Ocean: Spectra and Sources. *The Journal of the Acoustical Society of America*, 34(12):1936–1956, 12 1962.

[10] S. Matzner, A. Maxwell, J. Myers, K. Caviggia, J. Elster, M. Foley, M. Jones, G. Ogden, E. Sorensen, L. Zurk, J. Tagestad, A. Stephan, M. Peterson, and D. Bradley. Small vessel contribution to underwater noise. In *MTS/IEEE Seattle, OCEANS 2010*, MTS/IEEE Seattle, OCEANS 2010, 2010. MTS/IEEE Seattle, OCEANS 2010 ; Conference date: 20-09-2010 Through 23-09-2010.

[11] William M Carey. Lloyd's mirror-image interference effects. *Acoust. Today*, 5(2):14–20, 2009.

[12] European Commission. Quietmed – joint programme on noise (d11) for the implementation of the second cycle of the msfd in the mediterranean sea. `http://www.quietmed-project.eu/wp-content/uploads/2019/01/QUIETMED_D3.5_Best-practice-guidelines-on-continuous-underwater-noise-measurement_final.pdf`, march 2016.

[13] Łacny, Łukasz and Ścisło, Łukasz and Guinchard, Michael. Application of Probabilistic Power Spectral Density Technique to Monitoring the Long-Term Vibrational Behaviour of CERN Seismic Network Stations. *Vibrations in Physical Systems*, 31(3):2020311–1–2020311–7, 2020.

[14] Robert Lund, Hany Bassily, and Brani Vidakovic. Testing equality of stationary autocovariances. *Journal of Time Series Analysis*, 30(3):332–348, 2009.

[15] D. S. Coates and P. J. Diggle. Tests for comparing two estimated spectral densities. *Journal of Time Series Analysis*, 7(1):7–20, 1986.

[16] John G Proakis and Dimitris G Manolakis. *Digital signal processing*. Prentice-Hall, 1996.

[17] Varsha S. Amale, Shrikrishna U. Kolhar, Rajveer K. Shastri, and Arnab Das. Non-gaussianity and non-stationarity detection in underwater ambient noise using hypothetical tests. In *2016 Conference on Advances in Signal Processing (CASP)*, pages 270–275, 2016.

[18] Wenyan Wang, Jinming Wang, and Chaoqun Li. A signal detection method based on hybrid energy detection. In *2022 4th International Conference on Intelligent Control, Measurement and Signal Processing (ICMSP)*, pages 695–700, 2022.

Appendix A

Plots of the ESPRIT application

A.1 Plot of the simulation and tones detected by ESPRIT

The tones detected during a boat passage and during the usual noise using ESPRIT. As seen in figure A.1 the tones as well as the pattern of the tones are similar. Neither the corresponding relative amplitude in each application of the algorithm was useful in finding out if there was a boat, since these were close in size, usually about 0.98 out of the range between 1 and 0.

The parameters here, K and $dim(S+N)$, are set to 15 respective $2*K+2$. However, no significant effect was reached using $dim(S+N) = 100$. Probably, the combination of the parameters is important.

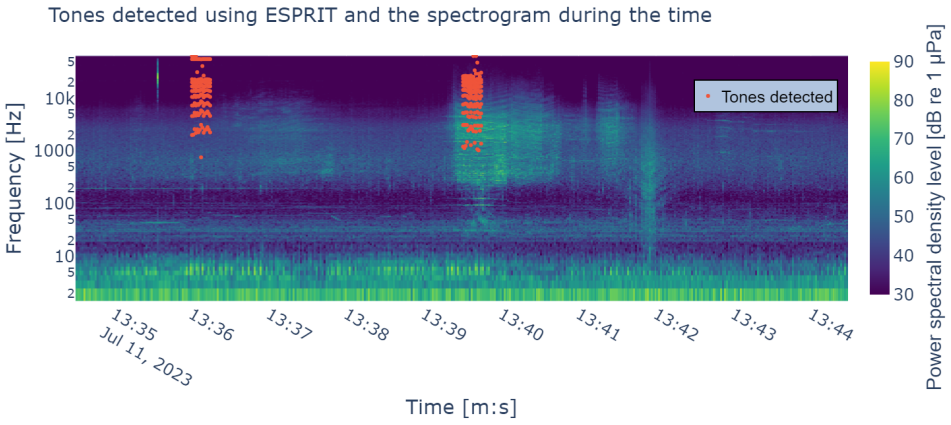

Figure A.1: The detected tones during a boat passage and during usual noise using ESPRIT.

The verification of the ESPRIT algorithm being correctly implemented is visible in figure A.2 below. The Fourier transform of the signal shows that there are 3

sinusoidal components. The parameters K and $dim(S+N)$ are set to 3 respectively 100.

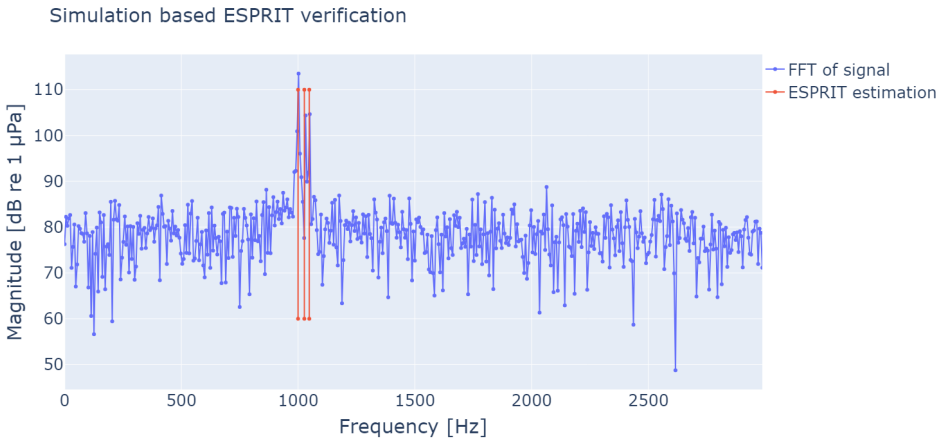

Figure A.2: The simulation of ESPRIT.

Appendix B

Plots for the bias removal

B.1 Plots of the average sound pressure values for different subwindow sizes

Here are the additional sensor plots for the bias removal investigation, except for sensor 6 which was not measuring at the time. The plots show the average values when using different subwindow sizes.

B.1.1 Sensor 1

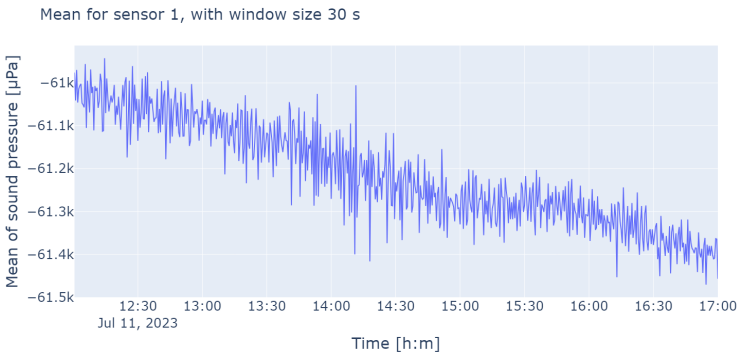

(a) The mean sound pressure using 30 seconds subwindows for sensor 1.

Figure B.1: The mean sound pressure using different subwindow sizes for sensor 1.

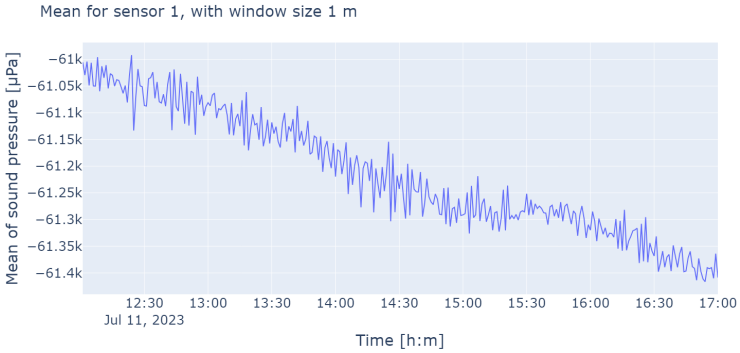

(b) The mean sound pressure using 1 minute subwindows for sensor 1.

(c) The mean sound pressure using 2 minutes subwindows for sensor 1.

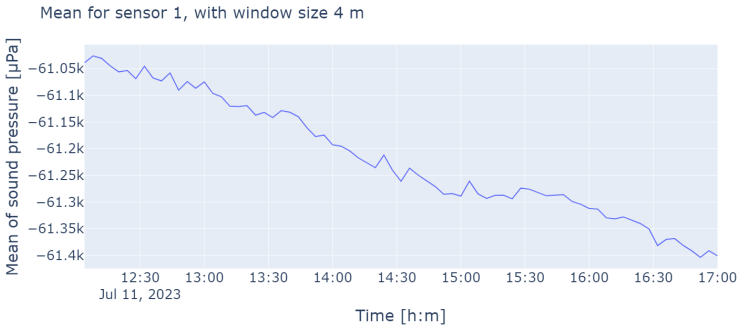

(d) The mean sound pressure using 4 minutes subwindows for sensor 1.

Figure B.1: The mean sound pressure using different subwindow sizes for sensor 1.

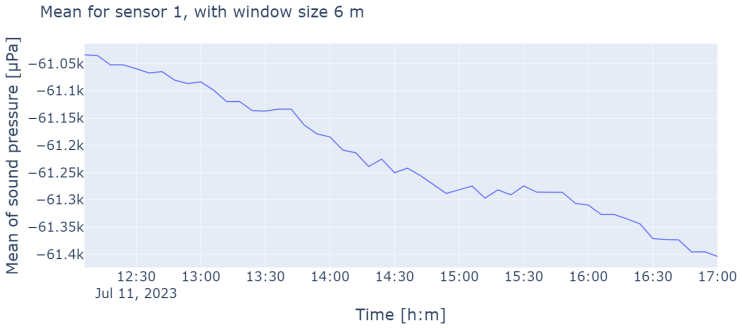

(e) The mean sound pressure using 2 minutes subwindows for sensor 1.

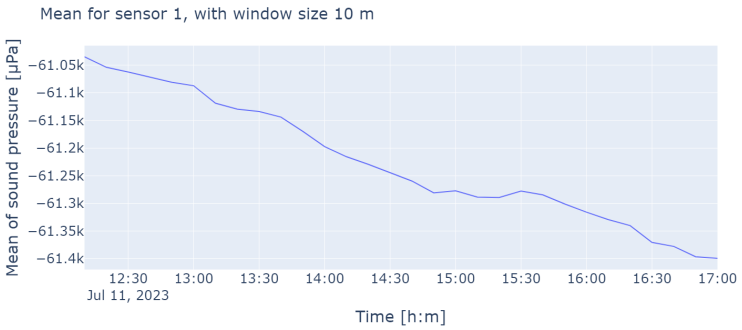

(f) The mean sound pressure using 10 minutes subwindows for sensor 1.

Figure B.1: The mean sound pressure using different subwindow sizes for sensor 1.

B.1.2 Sensor 2

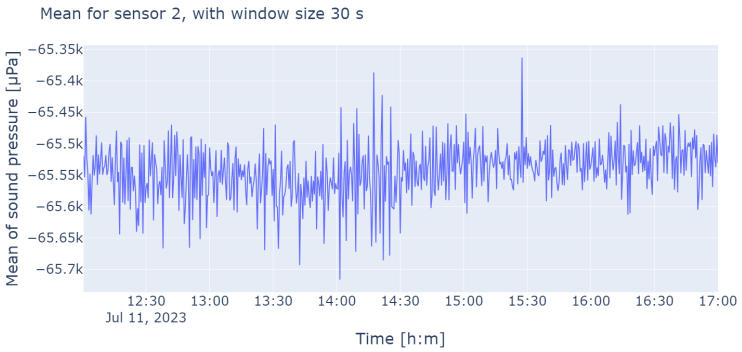

(a) The mean sound pressure using 30 seconds subwindows for sensor 2.

Figure B.2: The mean sound pressure using different subwindow sizes for sensor 2.

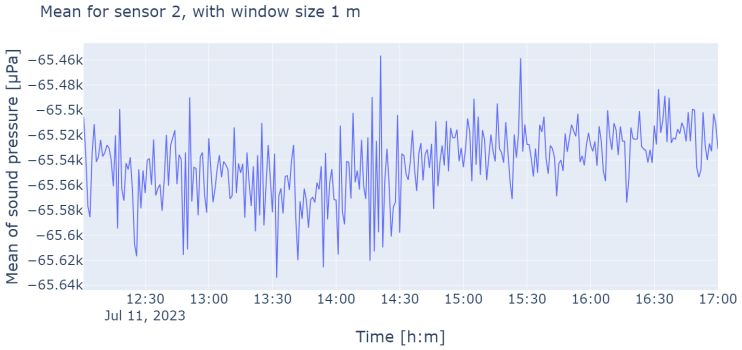

(b) The mean sound pressure using 1 minute subwindows for sensor 2.

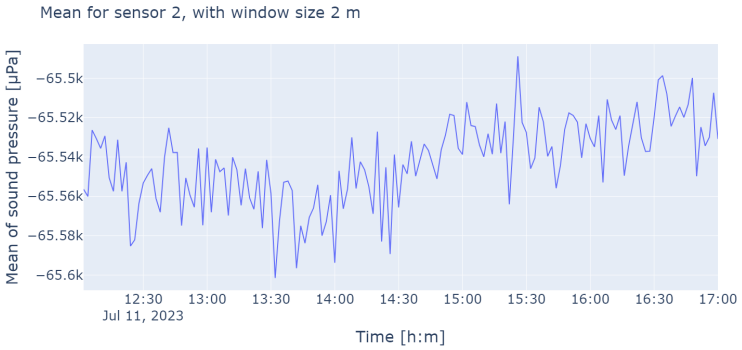

(c) The mean sound pressure using 2 minutes subwindows for sensor 2.

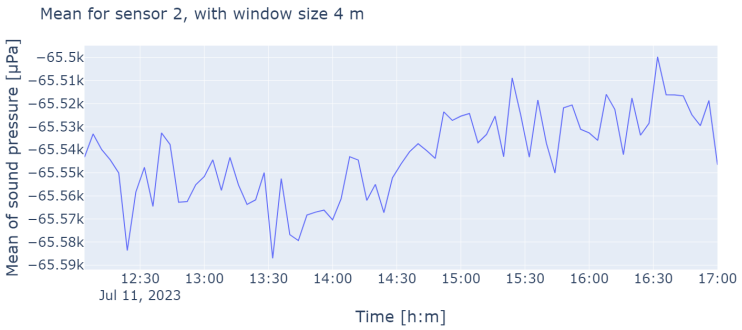

(d) The mean sound pressure using 4 minutes subwindows for sensor 2.

Figure B.2: The mean sound pressure using different subwindow sizes for sensor 2.

(e) The mean sound pressure using 6 minutes subwindows for sensor 2.

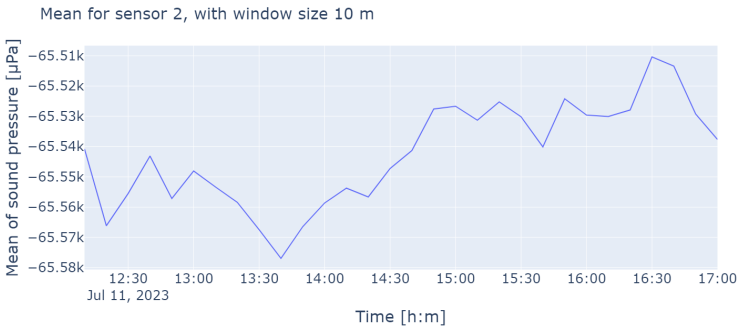

(f) The mean sound pressure using 10 minutes subwindows for sensor 2.

Figure B.2: The mean sound pressure using different subwindow sizes for sensor 2.

B.1.3 Sensor 3

(a) The mean sound pressure using 30 seconds subwindows for sensor 3.

Figure B.3: The mean sound pressure using different subwindow sizes for sensor 3.

(b) The mean sound pressure using 1 minute subwindows for sensor 3.

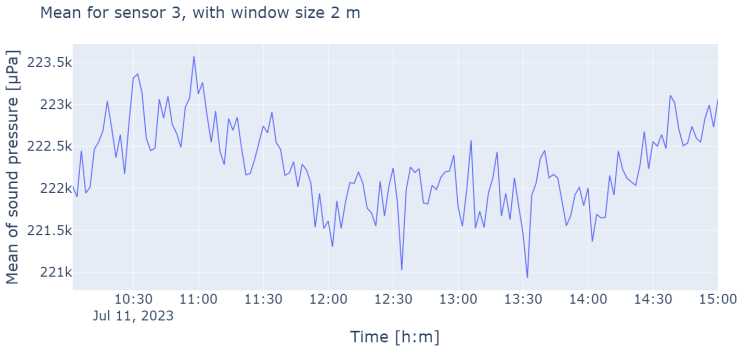

(c) The mean sound pressure using 2 minutes subwindows for sensor 3.

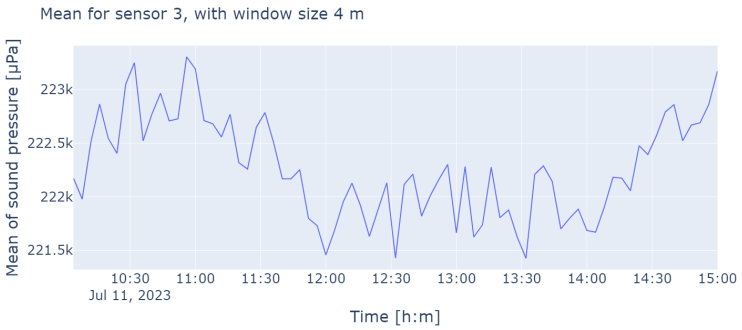

(d) The mean sound pressure using 4 minutes subwindows for sensor 3.

Figure B.3: The mean sound pressure using different subwindow sizes for sensor 3.

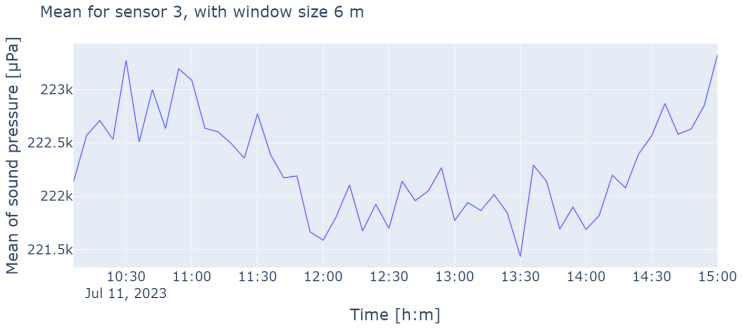

(e) The mean sound pressure using 6 minutes subwindows for sensor 3.

(f) The mean sound pressure using 10 minutes subwindows for sensor 3.

Figure B.3: The mean sound pressure using different subwindow sizes for sensor 3.

B.1.4 Sensor 4

(a) The mean sound pressure using 30 seconds subwindows for sensor 4.

Figure B.4: The mean sound pressure using different subwindow sizes for sensor 4.

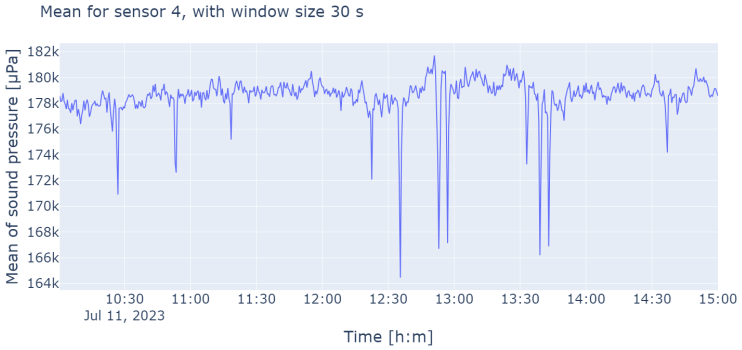

(b) The mean sound pressure using 1 minute subwindows for sensor 4.

(c) The mean sound pressure using 2 minutes subwindows for sensor 4.

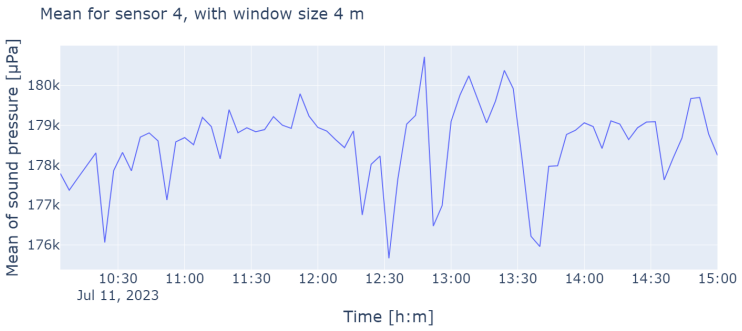

(d) The mean sound pressure using 4 minutes subwindows for sensor 4.

Figure B.4: The mean sound pressure using different subwindow sizes for sensor 4.

(e) The mean sound pressure using 6 minutes subwindows for sensor 4.

(f) The mean sound pressure using 10 minutes subwindows for sensor 4.

Figure B.4: The mean sound pressure using different subwindow sizes for sensor 4.

B.1.5 Sensor 7

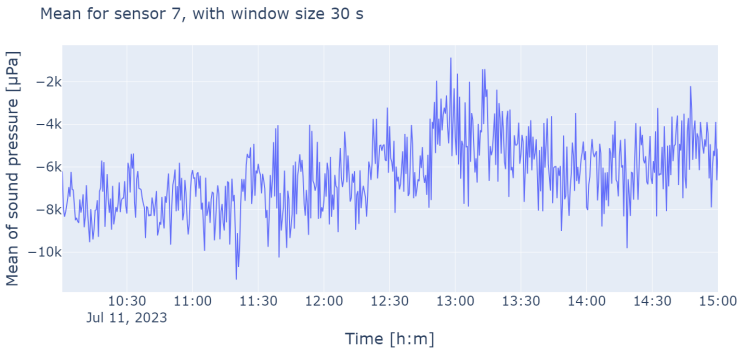

(a) The mean sound pressure using 30 seconds subwindows for sensor 7.

Figure B.5: The mean sound pressure using different subwindow sizes for sensor 7.

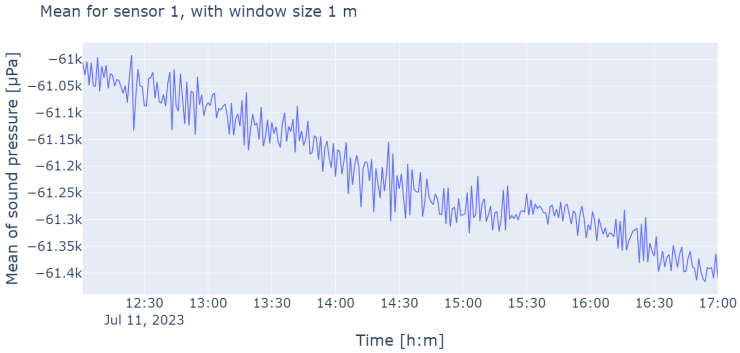

(b) The mean sound pressure using 1 minute subwindows for sensor 1.

(c) The mean sound pressure using 2 minutes subwindows for sensor 1.

(d) The mean sound pressure using 4 minutes subwindows for sensor 7.

Figure B.5: The mean sound pressure using different subwindow sizes for sensor 7.

(e) The mean sound pressure using 6 minutes subwindows for sensor 7.

(f) The mean sound pressure using 10 minutes subwindows for sensor 7.

Figure B.5: The mean sound pressure using different subwindow sizes for sensor 7.

Appendix C

Additional PPSD for boat noise contribution

The PPSDs for the night and the boat passages data for the additional sensors are shown below. The conclusions based on the analysis of the PPSDs in the following are equal to those in the chapter 5.

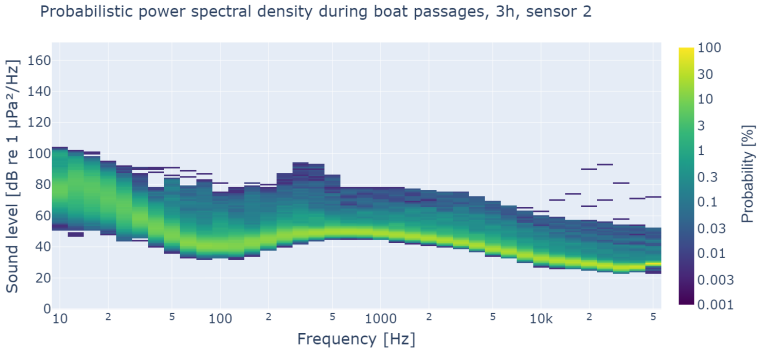

(a) The PPSD during 3 hours containing boat passages for sensor 2.

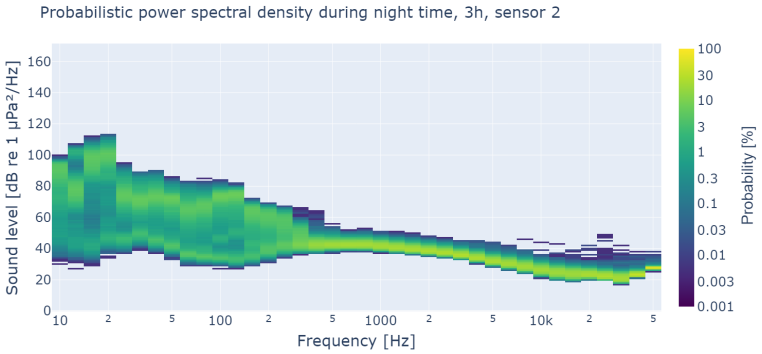

(b) The PPSD during 3 hours in the night for sensor 2.

Figure C.1: PPSDs during 3 hours, to give a sense of the boat noise contribution.

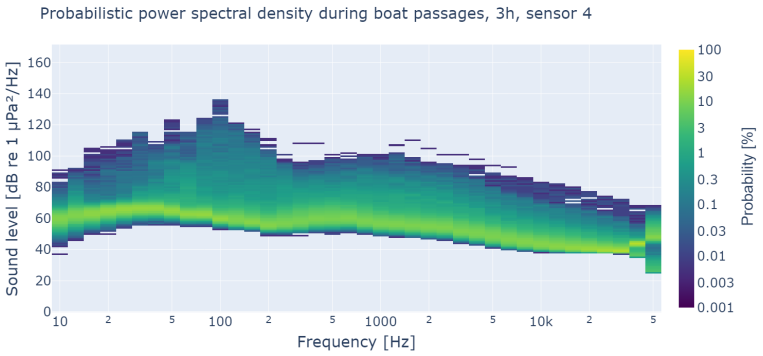

(c) The PPSD during 3 hours containing boat passages for sensor 4.

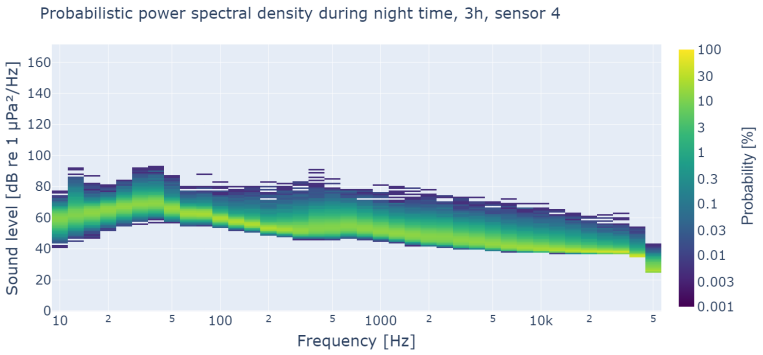

(d) The PPSD during 3 hours in the night for sensor 4.

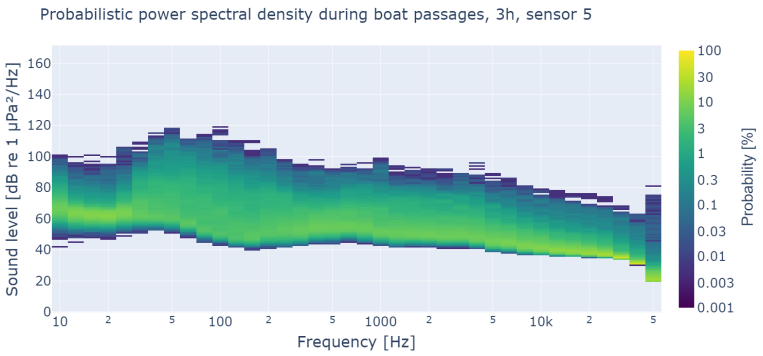

(e) The PPSD during 3 hours containing boat passages for sensor 5.

Figure C.1: PPSDs during 3 hours, to give a sense of the boat noise contribution.

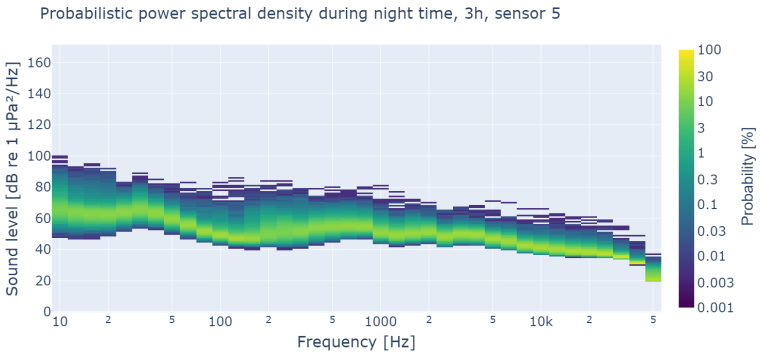

(f) The PPSD during 3 hours in the night for sensor 5.

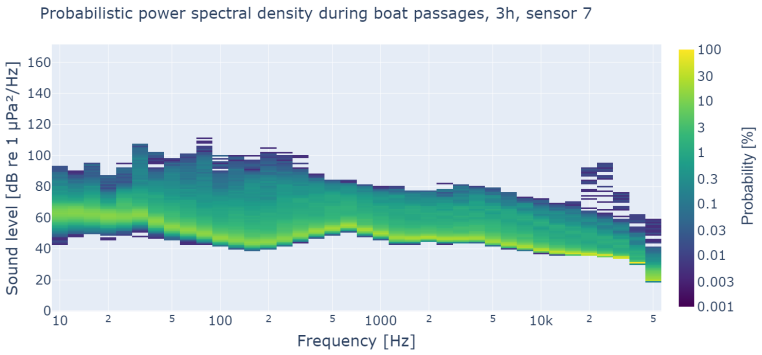

(g) The PPSD during 3 hours containing boat passages for sensor 7.

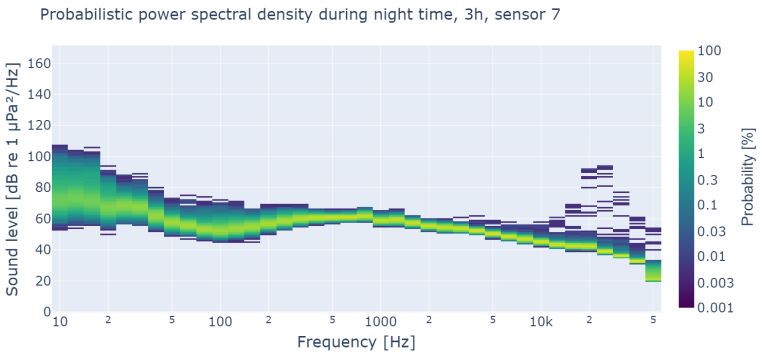

(h) The PPSD during 3 hours in the night for sensor 7.

Figure C.1: PPSDs during 3 hours, to give a sense of the boat noise contribution.

Appendix D

Plots for the energy detector

D.1 Plots for the different short subwindow sizes

Below the plots for the different short subwindow sizes. The application period also included precipitation at some sensor locations.

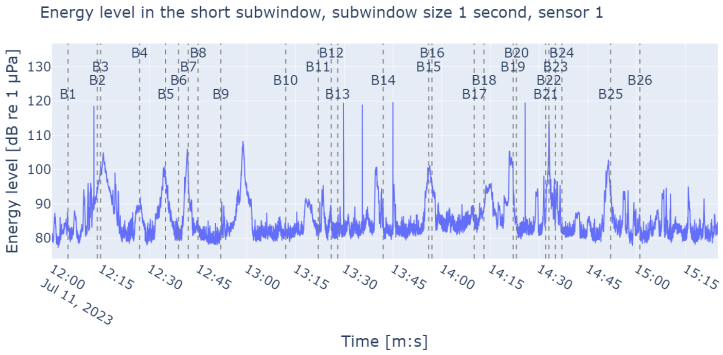

(a) The energy level of the short subwindow for subwindow size 1 second, sensor 1.

Figure D.1: The energy level of the short subwindows of different size, sensor 1.

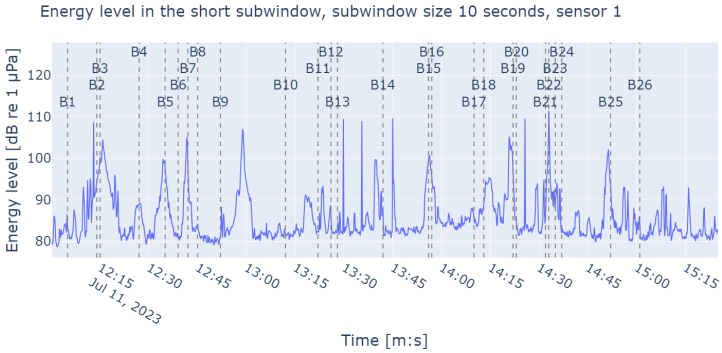

(b) The energy level of the short subwindow for subwindow size 10 seconds, sensor 1.

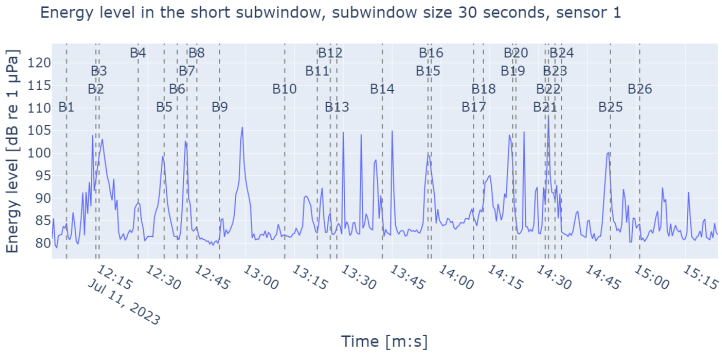

(c) The energy level of the short subwindow for subwindow size 30 seconds, sensor 1.

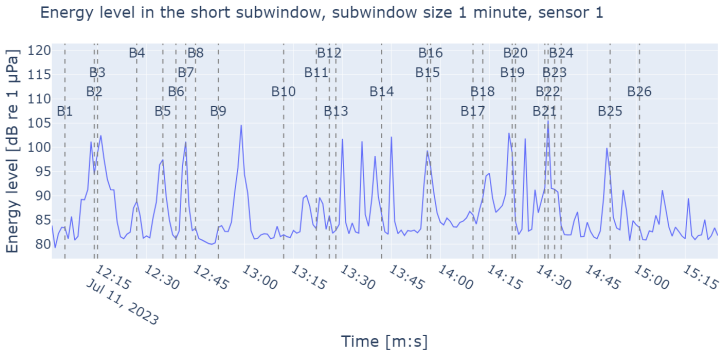

(d) The energy level of the short subwindow for subwindow size 1 minute, sensor 1.

Figure D.1: The energy level of the short subwindows of different size, sensor 1.

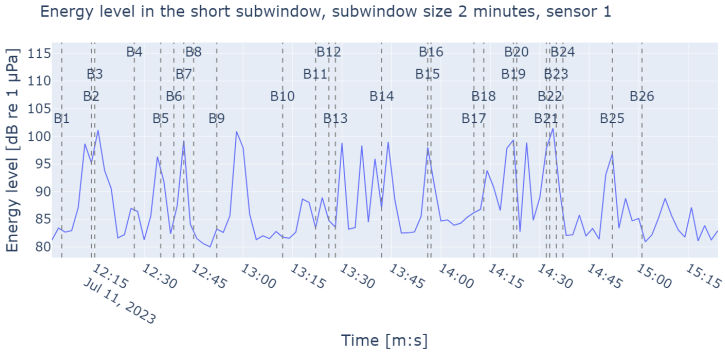

(e) The energy level of the short subwindow for subwindow size 2 minutes, sensor 1.

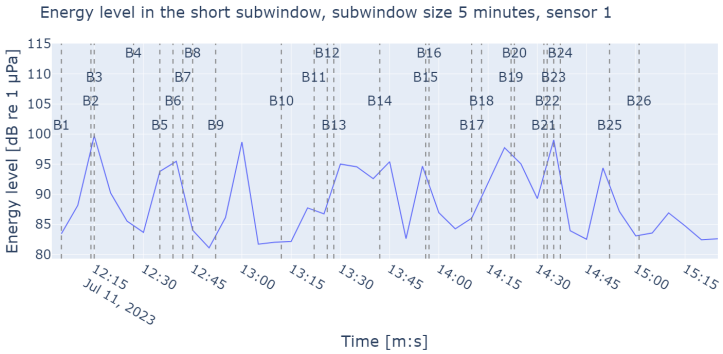

(f) The energy level of the short subwindow for subwindow size 5 minutes, sensor 1.

Figure D.1: The energy level of the short subwindows of different size, sensor 1.

D.1.1 Plots for the different short subwindow sizes during heavy precipitation

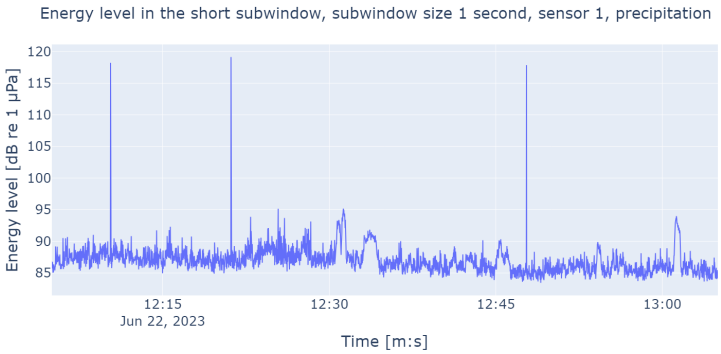

(a) The energy level of the short subwindow for subwindow size 1 second, sensor 1, precipitation.

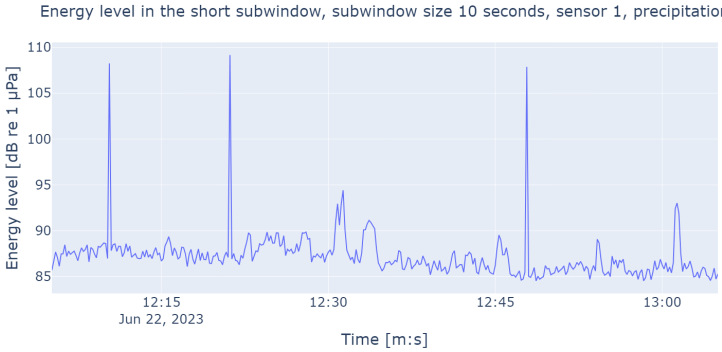

(b) The energy level of the short subwindow for subwindow size 10 seconds, sensor 1, precipitation.

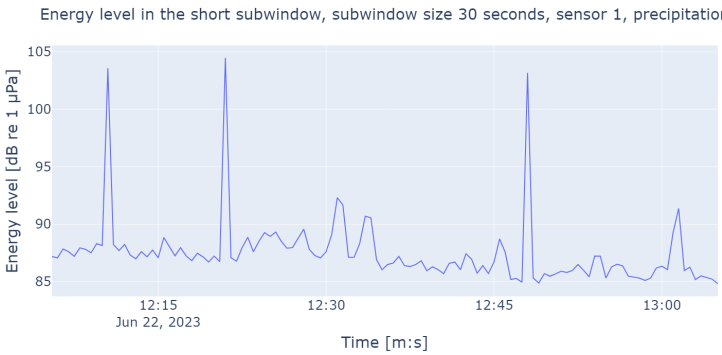

(c) The energy level of the short subwindow for subwindow size 30 seconds, sensor 1, precipitation.

Figure D.2: The energy level of the short subwindows of different size during precipitation, sensor 1.

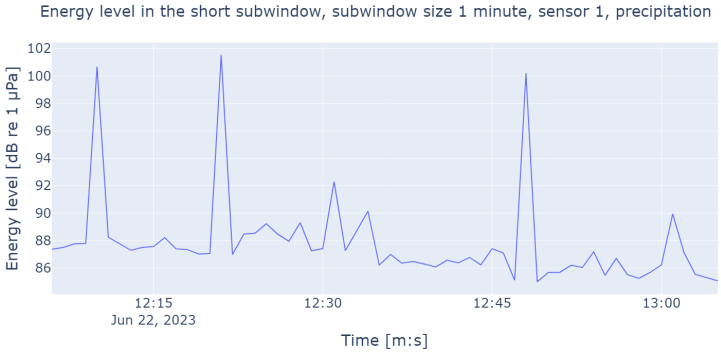

(d) The energy level of the short subwindow for subwindow size 1 minute, sensor 1, precipitation.

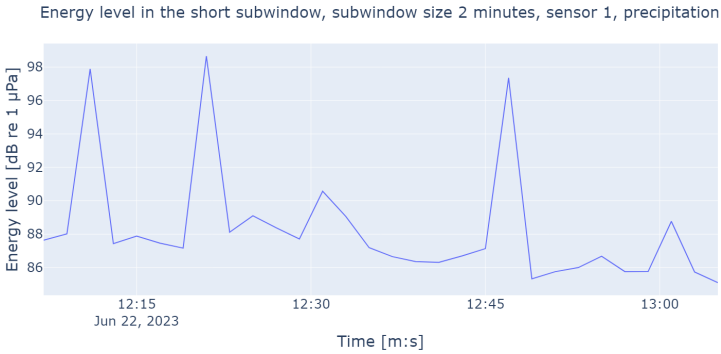

(e) The energy level of the short subwindow for subwindow size 2 minutes, sensor 1, precipitation.

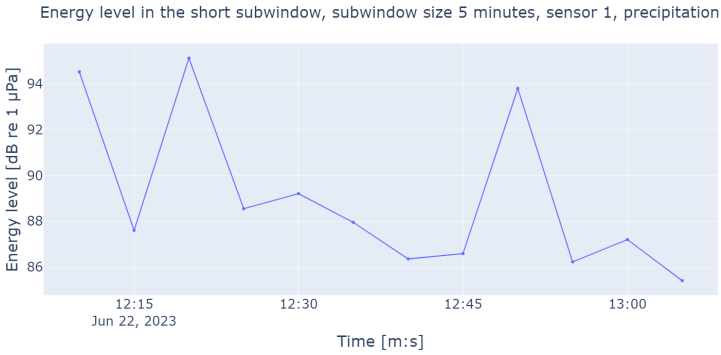

(f) The energy level of the short subwindow for subwindow size 5 minutes, sensor 1, precipitation.

Figure D.2: The energy level of the short subwindows of different size during precipitation, sensor 1.

D.1.2 The result of the detector when raining heavily

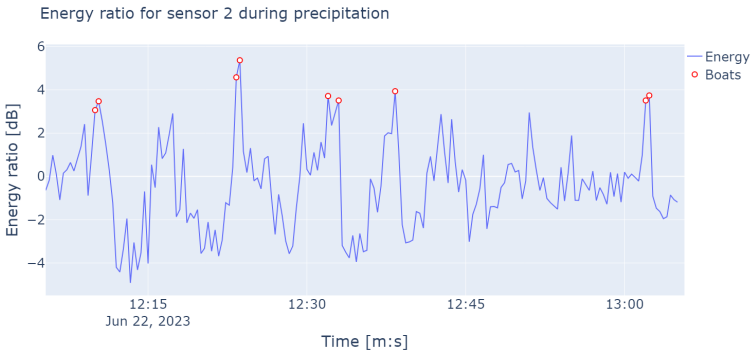

(a) The energy detection result for sensor 2.

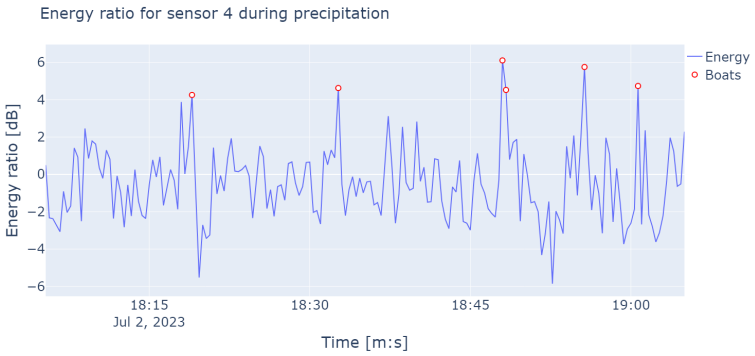

(b) The energy detection result for sensor 4.

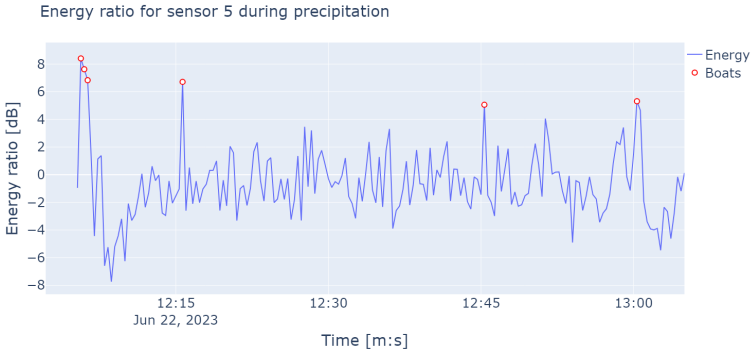

(c) The energy detection result for sensor 5.

Figure D.3: The energy detection result during precipitation.

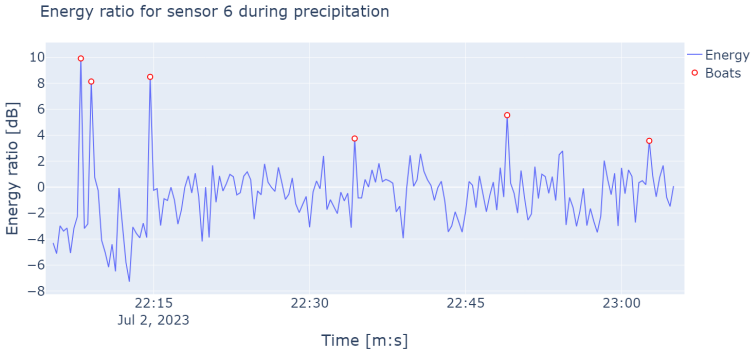

(d) The energy detection result for sensor 6.

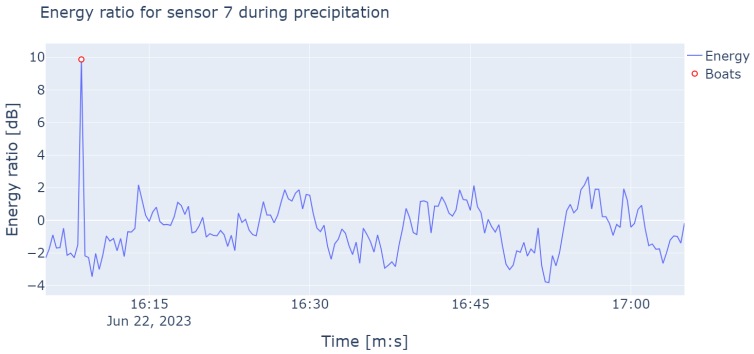

(e) The energy detection result for sensor 7.

Figure D.3: The energy detection result during precipitation.